Response to reviewers' reports on the paper acp-2018-1043 Simultaneous in-situ measurements of small-scale structures in neutral, plasma, and atomic oxygen densities during WADIS sounding rocket project

Boris Strelnikov[1], Martin Eberhart[4], Martin Friedrich[5], Jonas Hedin[3], Mikhail Khaplanov[3†], Gerd Baumgarten[1], Bifford P. Williams[6], Tristan Staszak[1], Heiner Asmus[1], Irina Strelnikova[1], Ralph Latteck[1], Mykhaylo Grygalashvyly[1], Franz-Josef Lübken[1], Josef Höffner[1], Raimund Wörl[1], Jörg Gumbel[3], Stefan Löhle[4], Stefanos Fasoulas[4], Markus Rapp[2], Aroh Barjatya[7], Michael J. Taylor[8], and Pierre-Dominique Pautet[8]

[1]Leibniz-Institute of Atmospheric Physics at the Rostock University, Kühlungsborn, Germany
[2]Deutsches Zentrum für Luft- und Raumfahrt, Institut für Physik der Atmosphäre, Oberpfaffenhofen, Germany
[3]Department of Meteorology (MISU), Stockholm University, Stockholm, Sweden
[4]University of Stuttgart, Institute of Space Systems, Stuttgart, Germany
[5]Graz University of Technology, Graz, Austria
[6]GATS, Boulder, USA
[7]Embry-Riddle Aeronautical University, FL, USA
[8]Center for Atmospheric and Space Sciences, Utah State University, Logan, Utah, USA
[†]Deceased

Correspondence: B. Strelnikov (strelnikov@iap-kborn.de)

We appreciate the reviewers' constructive comments and their positive judgment on our paper. We have taken the reviewers' suggestions into account when preparing the revised version of our manuscript.

In the following we address the comments of both reviewers point by point

(Every point contains: **Q:** reviewer's question, **A:** authors' answer, **T:** text from the revised manuscript).

To reviewer #1

1. **Q:** *Page 1, lines 12-13: 'GW might dissipate and thereby generate turbulence'-GW might break and generates turbulence. This statement can be supported by appropriate references of observational (e.g., https://doi.org/10.1002/2015JD024283) work(s) since a lot of studies are available but nothing cited.*

   A: As suggested by the reviewer, we added some references to observational works showing that breaking GW may generates turbulence.

   T: When propagating, GW might dissipate and thereby generate turbulence (e.g., Yamada et al., 2001; Selvaraj et al., and references therein).

2. **Q:** *Page 1, lines 13-14: 'Turbulence mixing and redistribution of trace constituents' can be supported by appropriate references of observational work(s).*

   A: We added some references were turbulence mixing and redistribution of trace constituents were studied experimentally

   T: Apart of the momentum deposition, which is a key coupling process, this also affects mixing and redistribution of trace constituents (e.g., Fukao et al., 1994; Bishop et al., 2004).

3. **Q:** *Page 2, lines 6-7: 'chemical heating rates in the mesopause region of several K/day which is comparable (or even competitive) to those of turbulent heating' can be supported by appropriate references of observational work(s) whos study concluded it statistically and/or mention case study.*

   A: As suggested, we supported the statement by references.

   T: These reactions yield chemical heating rates in the mesopause region of several K/day which is comparable (or even competitive) to those of turbulent heating (Mlynczak, 1996; Lübken, 1997; Lübken et al., 2002) as well as direct heating due to solar radiation (e.g., Fomichev et al., 2004; Feofilov and Kutepov, 2012; Lübken et al., 2013, and references therein).

4. **Q:** *Page 4, lines 23-25: It is stated in Page 3, lines 13-14 that 'MAARSY operated continuously to detect PMWE echoes if any' but no echo is detected during the night of rocket launch. It can be mentioned that echo occurrence depends on both nature of the target and sensitivity of the radar. It is better to reveal with help of volume reflectivity map (without any signal threshold) during that night of rocket launch. And select the profile of volume reflectivity to discuss the sensitivity of MAARSY at that time of sounding in MLT since this article deals with small scale dynamical fluctuations in densities while avoiding chemical reactions. It can be mentioned that during February-March 2011/2012 and 2012/2013, PMWE of MAARSY appeared throughout day and night with dis-continuities in seasonal- local time variation (see Fig. 3 of Latteck and Strelnikova, 2015).*

   A: As requested by the reviewer to better demonstrate the dynamic conditions for WADIS-2 rocket launch we added the plot of volume reflectivity measurements by MAARSY (see Fig. 2 below and in revised version of the manuscript). We also noted that the WADIS sounding rocket mission did not aim at studying radar echoes themselves, so that the presence of PMWE was not a criterion for rocket launch.

   T: Fig. 2 shows volume reflectivity measured by MAARSY during 5 of March, i.e. the day of the rocket launch. Some short-living echoes were observed around noon and in the late evening, but not in the morning when WADIS-2 rocket was launched. We recall here that this sounding rocket mission did not aim at studying PMWE, so that the presence of PMWE was not a criterion for rocket launch.

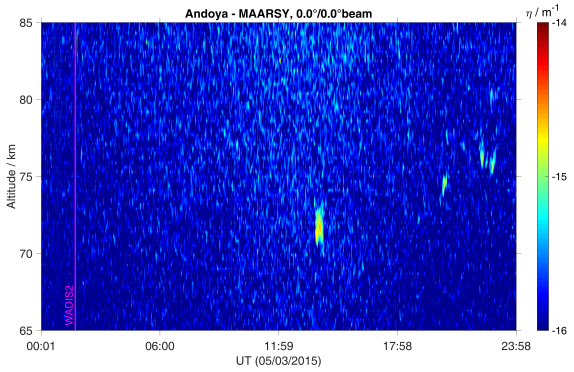

Figure 2. Volume reflectivity measured by MAARSY on 5 of March. Some short-living echoes were observed around noon and in the late evening but not around the WADIS-2 rocket launch.

5. **Q:** *Page 4, line 27: 'temperature field measured by the lidars'. Is it measured or estimated? If temperature is estimated then provide appropriate references to methodology for temperature retrieval which is used here*

   A: The reviewer is right that it was not explained in the paper how the temperature were measured by the lidars. We believe that lidars do measure temperatures, even though this may be considered as indirect measurements. Since we show measurement results of three different lidars, to address this reviewer's point we extended the section 2 (instrumentation) by an appropriate instrument descriptions and references.

   T: All three lidars measure temperatures profiles along the beam direction as shown in Fig. 1. The instruments and temperature retrieval techniques for these lidars are described elsewhere (von Zahn et al., 2000; Hauchecorne and Chanin, 1980; She et al.; Arnold and She, 2003; Höffner and Fricke-Begemann, 2005; Lautenbach and Höffner, 2004; Höffner and Lautenbach, 2009). Additionally, RMR- and Na-lidars measure line-of-sight wind speed in the altitude ranges 20–80 and 80–110 km, respectively (Baumgarten, 2010; Arnold and She, 2003).

6. **Q:** *Page 5: In Fig. 2, 'temperature of RMR- and Fe- lidar are combined'. How do they agree?*

   A: We added a short discussion to offer reader a guideline to estimate how the RMR- and Fe-lidar measurements agree.

   T: Fig. 3 utilizes measurements by the vertical beam of RMR-lidar since the mobile Fe-lidar only measures vertically. Also, the seeding temperature for derivation of RMR-temperatures was taken from Fe-lidar measurements. Signatures of long period waves are clearly seen above $\sim$65 km altitude in both RMR- and Fe-lidar measurements.

7. **Q:** *Page 5: In Fig. 2 and Fig. 3, It is better to limit the steps in colormap for easy reference of temperature in Fig. 2 and Fig. 3. And also provide temperature labels in colormap of Fig. 3. And show the results Fig.2 and Fig. without interpolation.*

   A: We changed the figures 2 and 3 as requested by the reviewer (Since we added an additional plot with radar measurements above, the numbering is increased by 1, i.e. see Fig. 3 & 4). The both figures do not contain any interpolation.

T: See Fig. 3 and Fig. 4.

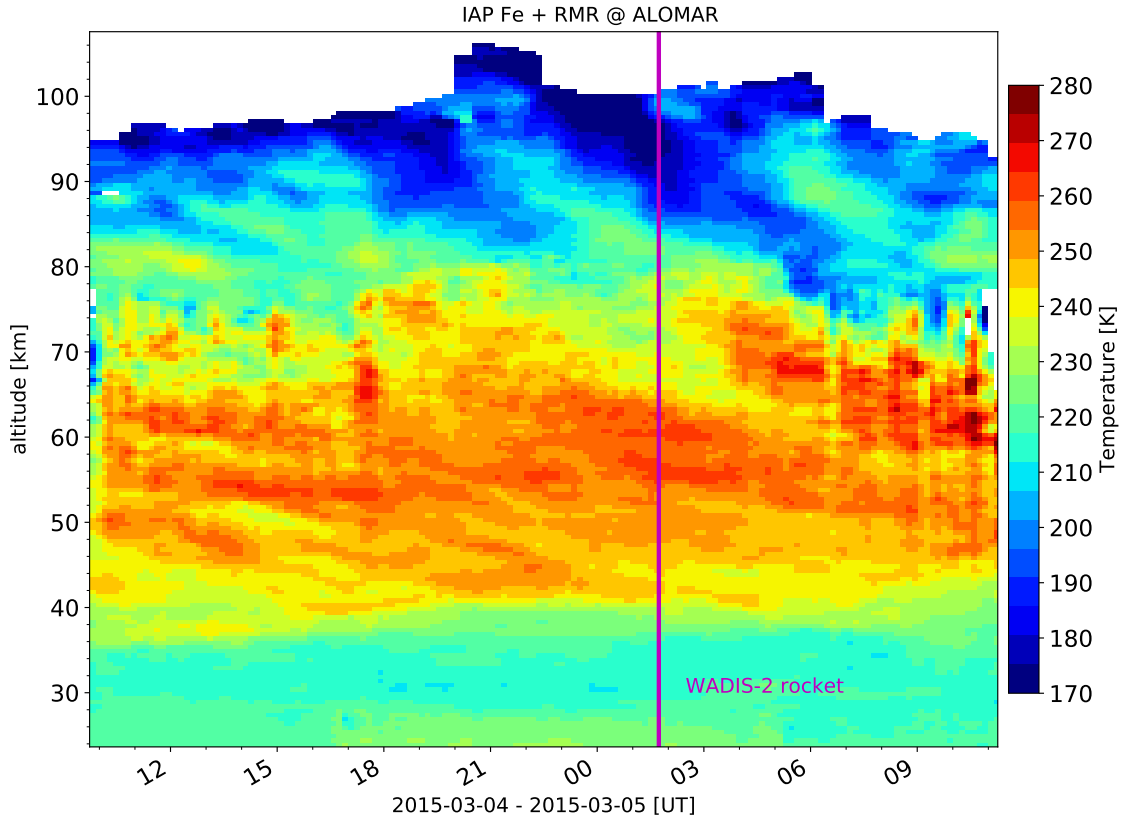

Figure 3. Combined RMR- and Fe-lidar temperature measurements during the night of the WADIS-2 rocket launch, i.e. 4 to 5 of March 2015.

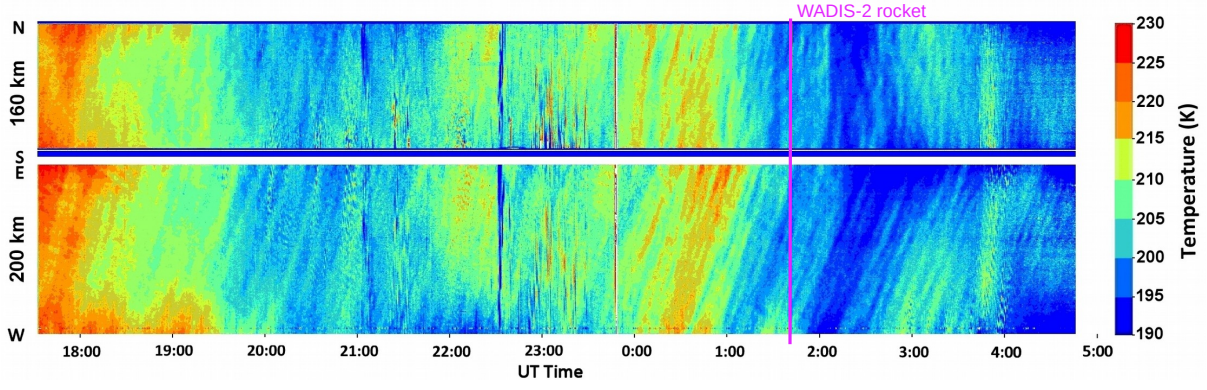

Figure 4. NS and WE keogram summary of the AMTM temperature measurements obtained during the night of 4 to 5 March 2015.

8. **Q:** *Page 7: In Fig. 5, Rocket observed densities are seem to be very much smoothed. How it is smoothed?*
   A: see next point

9. **Q:** *Page 7: In Fig. 5, Do you find any spin frequency in up- and down-leg of rocket observations? If yes, what are the methods are used to remove those frequency and what are they?*
   A: We added a description of how smoothing and spin filtering was applied to the rocket-borne density measurements.

   T: The spin frequency of WADIS-2 rocket of 3.27 Hz which modulated the raw data was filtered out by applying a notch filter. Additionally, the shown in-situ measured densities were smoothed by running average of a length of $\sim$200 m.

10. **Q:** *Page 7: Line 14, 'Both up- and down-leg profiles are very similar in terms of oscillations'. It is worth to show the detrended densities or density-normalised density fluctuations in subplot along with Fig. 5. item Page 7: Line 17, 'some GW-signatures'. It is better to quantify the GW amplitudes corresponding to Fig. 6, as you like, below 80 km, 83-90 km and 95-100 km.*
    A: Unfortunately, we do not really understand what reviewer means with the *"density-normalized density fluctuations"*. Our logical structure of the paper was as follows: first to described measurements as they were and then to make some analysis, in particular, extract fluctuations. According to this logic we show the relative density fluctuations in Fig. 10 (Fig. 11 in the revised version) in the section 4 "Analysis". As we understand, these relative fluctuations, i.e. the quantities $\Delta\rho/\overline{\rho} = (\rho - \overline{\rho})/\overline{\rho}$ (where ρ is measured density and $\overline{\rho}$ is a smoothed background density) are the *"density-normalized density fluctuations"* requested by the reviewer.
    The GW amplitudes are described as suggested.

    T: The temperature profiles clearly show some GW-signatures with amplitudes of up to 15 K at altitudes below 80 km. The height range between $\sim$83 and 90 km reveals very low GW amplitudes, i.e. temperature fluctuations of 1 K and less. A temperature increase of $\sim$40 K reminiscent of mesospheric inversion layers (MIL) similar to those analyzed by Szewczyk et al. (2013) is seen between 95 and 100 km and is discussed in Sec. 4. Some small-scale GWs with amplitudes between 1 and 5 K and vertical wavelength of the order kilometer are superposed on this large temperature disturbance.

11. **Q:** *Page 8: In Fig. 6, It is worth to describe the mothod(s) and along with valid assumptions used for temperature retrieval from densities. Include the profiles of temperature from Lidars in Fig. 6 for ready comparison of temperature osciallations between remote sensing and in-situ measurements.*
    A: We extended the instrumentation section with a description of derivation methods and underlying assumptions. Fig. 6 (Fig. 7 in the revised version) was changed and now includes profiles of lidar measurements.

    T: The measured density profile, in turn, can be integrated assuming hydrostatic equilibrium to yield temperature profile (see e.g., Strelnikov et al., 2013, for details).
    Fig. 7 additionally shows temperature profiles in magenta, yellow, and red measured by RMR-, Na-, and Fe-lidars, respectively.

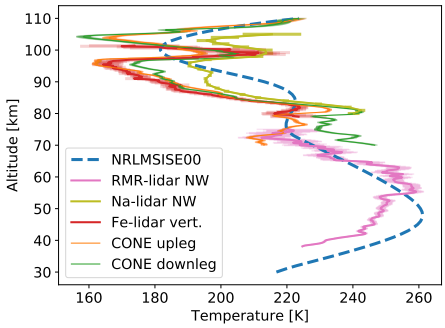

Figure 7. Temperatures derived from the densities shown in Fig. 6 assuming hydrostatic equilibrium.

12. **Q:** *Page 9: Line 1, 'some aurora was seen'. It is better to mention the wave length of those observed emissions.*
A: We extended the section 2 "Instrumentation" by a description of this photometer.

T: The second MISU photometer on the payload measured the emission from the (0-0) band of the N_2^+ 1st negative band system centered at 391.4 nm. This emission is a sign of precipitating auroral electrons and thus a sensitive indicator of auroral activity.

13. **Q:** *Page 9: Line 14, 'O-density profiles reveal some oscillations'. It is better to show profiles of density-normalised density fluctuations in subpot along with Fig. 8.*
A: see point 10 above.

14. **Q:** *Page 11: Fig. 10, It is better to have percentage of amplitude and densitynormalised density fluctuations in Fig. 10.*
A: We are convinced that wind fluctuations in absolute values (m/s) are more informative than those in percent. However, we put here the requested figure to show the reviewer how it looks in percent.
See also point 10 above.

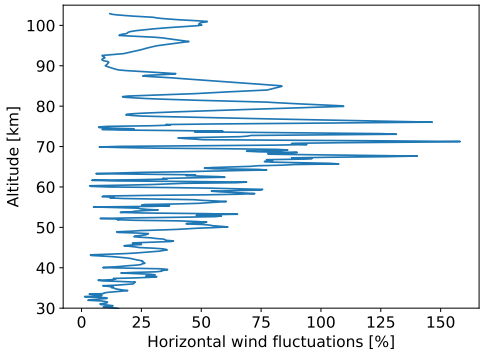

Figure 10. Horizontal wind fluctuations in percent.

15. **Q:** *Page 11: Line 9, Before comparison of results, describe the observed results of turbulence intensity from different techniques (Heisenberg and Tatarskii) to demostrate the need of different techniques here. And also present the mean of them in order to present quatification of turbulence intensity.*

A: The turbulence analysis technique utilized in this study is the same regardless of spectral model applied. The differences in derived energy dissipation rates arise due to numerous factors. A comparison of these differences and discussion of reasons and uncertainties is currently a subject of another paper we are working on and definitely lies out of the scope of this article. We decided to present both results (Heisenberg and Tatarskii) separately to thereby demonstrate and to allow the reader to get some filling of method uncertainties. The discrepancies of the ε-values derived from those two models increase when we derive mean values over extended altitude region. The presence of both Heisenberg and Tatarskii results separately, as well as the mean values over ten kilometers are shown for compatibility reasons, i.e. to enable their comparison with those used in other studies (e.g., Strelnikov et al., 2017; Szewczyk, 2015).

16. **Q:** *Page 12: Lines 6-7, 'This picture is reminiscent of a GW-saturation process when vertical wavelength of GW becomes shorter'. It is worth to quantify the GW activity using the lidar observations and compare them with Fig. 12 for quantitative and qualitative statements since this article mainly focus on dynamics of smallscales.*

A: The reviewer is absolutely right that it would be valuable to make an in depth quantitative analysis of the observed gravity waves (GW) and there parameters. We are currently working on a detailed analysis of GWs observed in the course of WADIS-2 campaign and we have realized, that the detailed picture is rather complicated. In particular, we believe that we observed a superposition of many "quasi-monochromatic" GWs, that we observed many different wave packets at different altitudes, etc. We are convinced that quantification of the observed wave parameters needs a careful detailed study which is not finished yet.

Another more in depth analysis is presented in paper by Wörl et al. (2019) which we mentioned in the manuscript.

That is why we decided to not aim at detailed analysis of gravity waves in this paper. Rather, as we stated in the beginning "This paper aims at two things. First, it is to provide an overview of the WADIS-2 sounding rocket campaign and measured parameters, and second, to demonstrate that gravity wave motions and turbulence effects distribution of atomic oxygen in the nighttime MLT region."

17. **Q:** *Page 13: Line 14, Briefly describe the assumptions behind this Heisenberg model and the value of its constants which is used in it. How those constants are obtained?*

A: We believe that by properly addressing this point we will victimize the readability of the manuscript and will loose the main focus of the paper. As we already mentioned answering the point 15 above, this point is a subject of another study that should be published in a nearest future. However, to address this referee's comment we expanded the section 2 "instrumentation" by a brief description of the turbulence derivation technique.

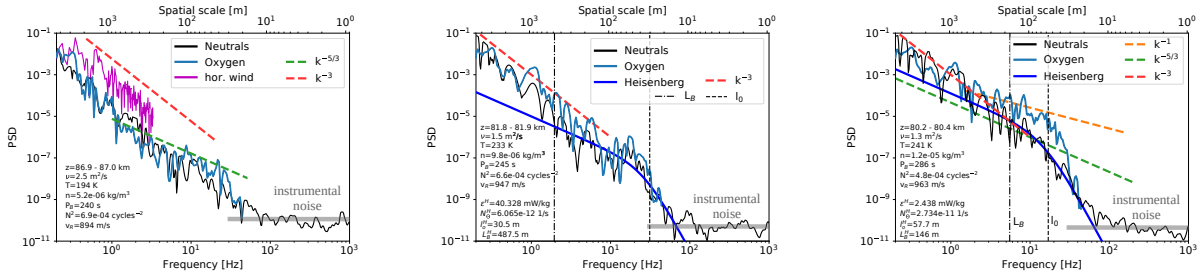

Figure 14. Normalized power spectral densities (PSD) of horizontal wind fluctuations (magenta), $\Delta N_n/N_n$ (black), and $\Delta[O]/[O]$ (blue) measured during descend of WADIS-2 sounding rocket. Dashed red, green, and orange lines show slopes with k^{-3}, $k^{-5/3}$, and k^{-1} power law, respectively. Vertical black dashed and dashed-dotted lines mark inner and buoyancy scales of turbulence, $l_\circ$ and L_B, respectively. Bold gray horizontal lines mark instrumental noise. a) All spectra reveal k^{-3} slope attributed to gravity waves; b) All spectra reveal both waves and turbulence. The neutral- and O-spectrum are near identical. c) Small-scale part of the O-spectrum reveal a k^{-1} slope.

T: The derivation technique of turbulent parameters is described in detail elsewhere Lübken (1992); Lübken et al. (1993); Lübken (1997); Strelnikov et al. (2003); Strelnikov et al. (2013). Briefly, a theoretical spectral model of turbulence is fitted to a Fourier or wavelet spectrum of the measured relative density fluctuations, which are shown to be a conservative and passive turbulence tracer in MLT (Lübken, 1992; Lübken et al., 1993; Lübken, 1997). The key-feature of this technique is that the theoretical model must reproduce spectrum of turbulent tracer (scalar) in both inertial (i.e. $\propto k^{-5/3}$) and viscous (or dissipation) subranges. Transition between these subranges takes place at the so called inner scale, l_0, which is related to the turbulence energy dissipation rate, ε as $l_0 = C(\nu^3/\varepsilon)^{(1/4)}$, where ν is the kinematic viscosity and the constant C is of the order 10. Also, Lübken et al. (1993) and Lübken (1997) showed that different spectral models, in particular those by Heisenberg (1948) and by Tatarskii (1971), yield close results of the energy dissipation rates.

18. **Q:** *Page 14: Fig. 13, Fig. 13a,b & c show the spectra of neutral densities in black line. In frequencies more than 100 Hz, neutral density fluctuations are appearing as almost flattened. Is this flattening due to instrumental noise? Indicate the instrumental noise as a line in Fig. 13a,b & c?*

A: Yes, the almost flat part of the spectrum in Fig. 13a, b, & c (Fig. 14a, 14b, & 14c in the revised version) is due to instrumental noise. We changed the figures as suggested by the reviewer and clarified it in the text.

T: The spectrum of the instrumental noise is marked in Fig. 14 by a bold gray horizontal line.

19. **Q:** *Page 15: Lines 1-2, '-value is directly derived from the spatial scale lo'. Provide the formulea and appropriate references along with valid assumptions and constants.*

A: This comment is addressed above in scope of point 17.

20. **Q:** *Page 15: Line 15, 'MIL descended together with tide'. Quantify the tidal activity using the lidar temperature measurements since demostrated examples behave very good.*

A: We believe that the reviewer means that we should quantify the tidal activity in WADIS-2 measurements, whereas that sentence refers to observations by Szewczyk et al. (2013). So, we addressed this point by answering the question 21.

21. **Q:** *Page 15: Lines 18-19, 'This temperature enhancement also descends within a time period of several hours'. Provide the descend rate.*

A: Provided as suggested.

T: Our temperature enhancement (compare Fig. 7 and 3) also descends within a time period of several hours. Their temporal behavior is studied in Wörl et al. (2019), who found dominant periods of 24, 12, and 8 hours.

22. **Q:** *Page 15: Line 20, 'The upleg rocket data, however, are somewhat different'. What are the differences are observed and at what altitude?*

A: We changed the wordings to make it clear that the temperature enhancements on up- and downleg are similar, turbulence is only strong in the downleg data.

T: The upleg rocket data, however, are somewhat different. While the upleg measurements show similar temperature enhancement, the turbulence observed is one order of magnitude weaker.

23. **Q:** *Page 15: Line 22, 'MIL, it might have amplified it'. what are the sources might cause amplification of MIL at this altitude (provide appropriate references also)?*

A: Szewczyk et al. (2013) argued that very strong turbulence could increase temperature enhancement associated with MIL by direct frictional heating effect produced by turbulence. This statement was not a confirmed fact deduced from measurements, but rather as a suggested interpretation which was consistent with observations.

24. **Q:** *Page 15: Line 23, 'The weaker turbulence on upleg accompany â´Lij10 K colder temperature maximum'. I could not understand this. Can you rewrite it to make understanding in simple way.*

A: We rewrote the sentence to make it understandable.

T: The local temperature maximum near 100 km reveal $\sim$10 K lower values for upleg measurements than for downleg (see Fig. 7). Also turbulent energy dissipation rates measured on upleg show $\sim$one oder of magnitude lower values than those observed during rocket descend (Fig. 12).

25. **Q:** *Page 15: Line 26-27, 'First, the amplitudes of GW in these tracers are different. Second, the phases can be shifted relative to each other'. Can you provide values and discuss it? Since you have unique observations.*

A: See our answer on reviewer's comment 16.

26. **Q:** *Page 15: Lines 31-32, 'the neutral and ion density fluctuations must be in antiphase'. Is it possible to quantify the angle between neutral and ion fluctuations (< a, b >= |a|.|b|.cos(angle)) for those three altitudes or altitude regions*

where coherence exist? Then, Provide the quantification of those results and discuss them.

A: See our answer on reviewer's comment 16.

27. **Q:** *Page 16: Lines 6-7, 'where all three species, i.e. oxygen, ions, and neutrals show nearly the same oscillations'. It can be discussed based on quantified angles.*

    A: See our answer on reviewer's comment 16.

28. **Q:** *Page 17: Line 35, 'the k-1 slope at scales smaller than those where k-5/3 is present'. Provide the profiles of outer scale and inner scale as like" and indicate the altitudes in it where the spectral slope is seen as k-1. It provides the active altitude regions where two different type of diffusions take place since it is a unique measurements to deal with. And also compare these turbulence parameters with the same of low-latitude turbulence parameters since day-time low-latitude mesospheric turbulence measurements not have any affect with dusty plasma.*

    A: By trying to address this reviewer's comment we realized that due to very high intermittency of the observed turbulence field, marking regions with different types of spectra makes figures extremely crowded and absolutely not readable. So, we decided to comment on it in the text.

    We also believe that comparison with low-latitude turbulence parameters better fits to our newest data from recent sounding rocket campaign "PMWE" conducted in April 2018. One of the reason for that, that additionally to the rocket data we also have radar measurements, which makes it better comparable with the low-latitude measurements.

    T: Detailed analysis of all the regions where different types of O-density spectra occur is rather difficult because of different reasons. One reason is that when turbulence is very strong, its spectrum extends down to scales below current FIPEX resolution limit of $\sim$20 m, that is the O-density spectrum appears not fully resolved. So far we can only identify three regions where third type of spectra (like in Fig. 14c) was observed in the downleg measurements: between 90.9–91.2 km, 80.2–80.4 km, and 81.1–81.7 km.

29. Other minor corrections made as requested.

To reviewer #2

1. **Q:** *Page 2 line 8: provide citation for turbulent and solar heating rates.*
   A: Provided as requested.

   T: direct heating due to solar radiation (e.g., Fomichev et al., 2004; Feofilov and Kutepov, 2012; Lübken et al., 2013, and references therein).

2. **Q:** *Page 4 line 7: FIPEX - define acronym*
   A: Done.

   T: FIPEX stands for „Flux-Probe-Experiment“,...

3. **Q:** *Page 4 line 9: Could you give a brief description of this technique?*
   A: As suggested by the reviewer, we extended the section 2 "instrumentation" by a short description of this measurement technique.

   T: FIPEX stands for „Flux-Probe-Experiment“, it employs solid electrolyte sensors having gold electrodes with selective sensitivity towards atomic oxygen. A low voltage is applied between anode and cathode pumping oxygen ions through the electrolyte ceramic (yttria stabilized zirconia, YSZ). The current measured is proportional to the oxygen flux. A detailed description of measurements conducted by FIPEX during WADIS mission is provided by Eberhart et al. (2015) and Eberhart et al. (2018) for the first and second campaign, respectively.

4. **Q:** *Figure 2: How are the RMR and Fe lidar data combined? What is the direction of these measurements?*
   A: We expanded the description of the lidar measurements by addressing this comment of the reviewer.

   T: Fig. 3 utilizes measurements by the vertical beam of RMR-lidar since the mobile Fe-lidar only measures vertically. Also, the seeding temperature for derivation of RMR-temperatures was taken from Fe-lidar measurements.

5. **Q:** *Section 3.2, second paragraph: mention in the text (not just in the figure caption) which instrument was used to derive the total number density and temperature profiles and how the temperatures are derived from the densities.*
   A: To address this comment of the reviewer we extended the section 2 "instrumentation" by a short description of the absolute density and temperature derivation technique by the CONE instrument. Also, we mentioned in the text that the shown densities and temperatures were measured in-situ by the CONE instrument.

   T: CONE measures density of neutral air with altitude resolution of $\sim$30 cm. Making use of laboratory calibrations allows to derive absolute density altitude-profile. The measured density profile, in turn, can be integrated assuming hydrostatic equilibrium to yield temperature profile (see e.g., Strelnikov et al., 2013, for details).

   Figs. 6 and 7 show profiles of neutral air densities and temperatures measured in-situ by the CONE instrument.

6. **Q:** *Page 8 paragraph 2: What are the values of the ionospheric parameters used in the IMAZ model to produce the profile in Fig. 7?*

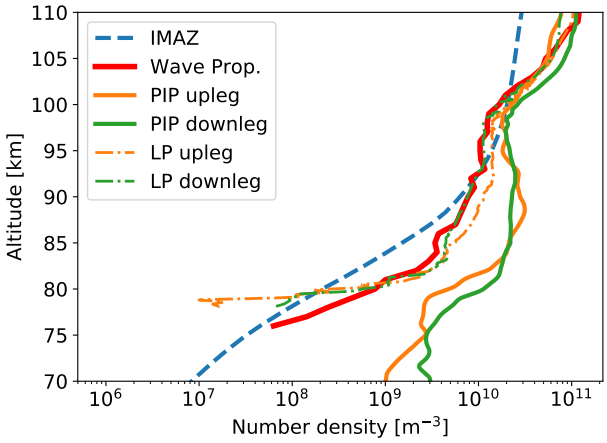

Figure 8. Densities of positive ion (solid orange and green lines) and electron (dash-dotted orange and green profiles) densities measured by the PIP and LP instruments, respectively. Bold solid red line shows results of the wave propagation experiment. Blue dashed line shows electron density from the empirical ionospheric model for the auroral zone, IMAZ, derived for the time of the WADIS-2 flight (see text for details).

A: As suggested by the reviewer, we added description of inputs for the IMAZ model. Additionally, we added profile of the absolute electron densities measured by the radio wave propagation experiment to the Fig. 7 (Fig. 8 in the revised version).

T: The inputs for IMAZ model are F10.7 solar flux index of 137.9 Jy (1 Jy = 10^{-26} W m^{-2}Hz^{-1}), the planetary magnetic Ap index 5, and riometer absorption @ 27.6 MHz of 0.076 dB. Activity indices, the solar F10.7 and Ap index, were obtained from the GSFC/SPDF OMNIWeb interface at https://omniweb.gsfc.nasa.gov. The integral riometer absorption was estimated from the electron density measurements by wave propagation experiment based on Friedrich and Torkar (1983).

7. **Q:** *"This is in accord with the fact that some aurora was seen" - by what instruments? "auroral emission detector. . . registered some auroral emission above 100 km" - how does this instrument work, what is measured? It might be useful to add this instrument to your list of rocket instruments in Sect. 2. Could you quantify "some auroral emission"?*

A: As suggested by the reviewer, we added both brief description of this instrument in section 2 "instrumentation" and short description of the measured quantity.

T: Section 2: The second MISU photometer on the payload measured the emission from the (0-0) band of the N_2^+ 1st negative band system centered at 391.4 nm. This emission is a sign of precipitating auroral electrons and thus a sensitive indicator of auroral activity.

Section 3: The overhead emission seen by the second MISU photometer was varying (both increasing and decreasing at times) during the flight indicating that the auroral emission was variable in time. The auroral emission was relatively weak with peak total band radiances of 700–800 Rayleighs (around $6 \cdot 10^7$ photon $\cdot$ s^{-1} str^{-1} cm^{-2}).

8. **Q:** *Page 9, line 3: "The shown plasma density profiles yield relative density measurements and therefore they were normalised. . ." This sentence seems to be the wrong way around: do you mean the measurements yield relative quantities that are therefore normalised to produce the profiles in Fig. 7? If so, this could also be mentioned in the caption.*

A: To avoid the misunderstanding we have rephrased this paragraph.

T: The PIP and LP instruments yield measurements of relative densities of positive ions and electrons, respectively. The wave propagation experiment yields accurate measurements of absolute electron densities, which are used to normalize the PIP- and LP-measurements. The normalization was made at an altitude of $\sim$115 km, where quasi-neutrality condition is well satisfied for ionospheric plasma (see e.g., Friedrich, 2016; Asmus et al., 2017, for more details).

9. **Q:** *Figures 5, 7, and 8: Please use consistent units: m-3 is used in Figs. 5 and 7, and cm-3 is used in Fig. 8.*

A: Fig. changed as suggested.

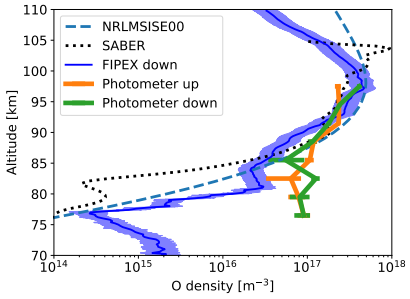

Figure 9. Atomic oxygen densities measurements. Bold orange and green lines with error-bars show photometer measurements on up- and downleg, respectively. FIPEX downleg data is shown by blue profile with shaded area showing measurement errors. Black dotted line shows SABER measurements (Level 2A, O event 20 orbit 71729). Blue dashed line shows NRLMSISE-00 model data for the time of rocket launch.

10. **Q:** *Figures 7 and 8: In the captions, I am not sure I see what is the "same as Fig. 5", except that these are atmospheric density profiles, but they are from different species, measured by different instruments!*

    A: Corrected as suggested.

11. **Q:** *Figure 7: What is the quantity plotted from the IMAZ model? Is it ion or electron density?*

    A: We improved both text and figure caption to make it clear, that we show electron density profile derived from the IMAZ model.

    T: Comparison with the electron density profile from the empirical ionospheric model for the auroral zone, IMAZ (McKinnell and Friedrich, 2007) shown in Fig. 8 (blue dashed line) shows that ionization level of the ionosphere was moderately high. This is in accord with the fact that some aurora was seen throughout the night of these observations.

    Fig. caption: Blue dashed line shows electron density from the empirical ionospheric model for the auroral zone, IMAZ, derived for the time of the WADIS-2 flight (see text for details).

12. **Q:** *Page 9 paragraph 2: I think you need to provide more details on the FIPEX instrument (either here or in Sect. 2). Could you specify why you are "mostly confident" in the descending data but not the ascending? Is this through comparison with data from the MISU photometers? Do you have an explanation as to what might be causing FIPEX to give erroneous measurements during one phase of the rocket flight but not another?*

    A: To address this reviewer's comment we added a paragraph with brief explanation. We do not want to go in more details since they are discussed in the companion paper by Eberhart et al. (2018) in this special issue. The short story is that the FIPEX is sensitive to incoming flow because its current ultimately depends on incoming flux of the atomic oxygen. In combination with the limited time constant of the FIPEX it can result in that under unfavorable (rapidly varying) aerodynamic conditions (i.e. rapidly changing influx of O) FIPEX may somewhat underestimate the absolute value of the ambient O-density.

    T: We note here that the FIPEX is a new instrument which was first applied for oxygen density measurements on sounding rockets during WADIS-1 rocket campaign (Eberhart et al., 2015). It showed good results and demonstrated principal possibility of a high resolution O-density measurements in MLT. WADIS-2 rocket was additionally equipped with the MISU airglow photometer that indirectly measures O-density from emission of the molecular oxygen Atmospheric Band. Such type of measurements is widely used also from the ground- or satellite-based platforms and is commonly accepted as reliable. The WADIS-2 sounding rocket comprised the both measurement techniques on the same platform which made it possible to closely compare their results. The both WADIS payloads (i.e. for the first and second campaigns) were equipped with several FIPEX sensors which were mounted at different angles relative to rocket velocity (or rocket symmetry) axis. Such multiple configuration aimed at finding the most favorable aerodynamic orientation for the FIPEX sensors. We also note that because of the supersonic rocket velocity the measurement results of most instruments on board sounding rockets require an aerodynamic correction (Gumbel et al., 1999; Gumbel, 2001; Rapp et al., 2001; Hedin et al., 2007; Staszak et al., 2015). By analyzing measurement conditions and comparing the measurement results we

chose the best quality FIPEX data for further analysis. For the detailed discussion of all FIPEX measurements the reader is referred to the companion paper by Eberhart et al. (2018).

13. **Q:** *Page 9 line 12: Are you linking the increase in oxygen density seen by SABER above 100 km to auroral activity because of the auroral emission measured at these altitudes by the rocket-bourne MISU instrument? If so, why is a similar increase not seen in the FIPEX oxygen measurements taken at the same location as those from the MISU instrument?*

    A: The reviewer is absolutely right that we link the increase in oxygen density seen by SABER above 100 km to auroral activity only based on the MISU auroral photometer observations. We added a sentence to note that the measurement principle of the FIPEX is based on direct sensitivity to the ambient O-concentration. Also, by addressing the reviewer's comments 2 and 3 we added a brief description of the FIPEX measurement technique in section 2. All those additions will make it clear that the FIPEX is insensitive to any emissions.

    T: We recall that the measurement principle of the FIPEX instrument is only sensitive to ambient O-density and does not react on emissions.

14. **Q:** *Page 9 paragraph 3: Again, a little more information on what the "other FIPEX sensors" measure would be helpful!*
    A: We believe that by addressing the point 12 of the reviewer we also clarified (answered) this comment.

15. **Q:** *Page 10 line 6: "small-scale stuff": colloquialism, please rephrase*

    A: Changed as suggested.

    T: For the small-scale structures in MLT and, especially those produced by turbulence,...

16. **Q:** *Page 10 paragraph 3: please specify which data are used to determine the fluctuations in Fig. 10; are these up or down leg measurements?*

    A: We clarified this point in both text and figure caption.

    T: These fluctuations were derived from the density profiles measured on the downleg of WADIS-2 rocket flight.

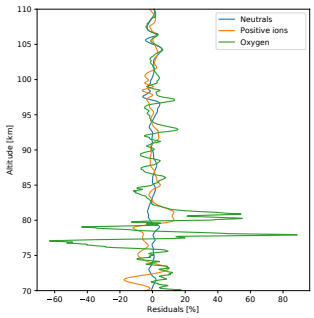

Figure 10. Relative density fluctuations (=residuals) of neutral air, positive ions, and atomic oxygen shown by blue, orange, and green profiles, respectively. These fluctuations were derived from the density profiles measured on the downleg of WADIS-2 rocket flight by subtracting a running average over 5 km long vertical window.

17. **Q:** *Fig. 11: provide the references for the turbulence climatologies in the text (not just the figure legend)*

A: Provided as suggested.

T: The black bold and grey profiles show climatologies, that is mean seasonal values for winter (Lübken, 1997) and summer (Lübken et al., 2002), respectively.

18. **Q:** *Page 11 line 7: "Also the upleg and downleg turbulence data qualitatively agree with each other." they do not agree below 70 km.*

A: We agree with the reviewer, that downleg measurements below 70 km are different. We discussed this difference further below in the text. However, we accept that to avoid confusion in has to be clearly stated already at this point.

T: Also the upleg and downleg turbulence data qualitatively agree with each other except small region observed between 63 and 67 km on downleg.

19. **Q:** *Page 11 line 9: "If compared with results of our previous rocket campaign WADIS-1 that was conducted in summer (Strelnikov et al., 2017), the observed winter turbulence field does not show big difference between up- and downleg measurements." It would be helpful to expand a little here and give (maybe just a sentence) on the WADIS-1 turbulence field.*

A: As suggested by the reviewer, we added a short summary on turbulence variability as found during WADIS-1 summer campaign.

T: Turbulence filed in summer MLT observed during WADIS-1 campaign showed large oscillations in both space and time so that even mean ε-values of up- and downleg rocket measurements differed by order of magnitude (Strelnikov et al., 2017). Turbulence variability in time was studied by analyzing MAARSY and EISCAT (European Incoherent SCATter Scientific Association) radar measurements which were properly scaled based on in-situ data. The MAARSY is only capable of measuring MLT parameters if some radar echo occurs, that is it needs presence of PMSE or PMWE. PMSE occurrence rate as observed by MAARSY is close to 100 % (Latteck and Bremer, 2017) which makes it easy to study MLT in summer season. The winter echoes, PMWE, are much more rare, i.e. their occurrence rate is at most 30 % (Latteck and Strelnikova, 2015).

20. **Q:** *Page 12 line 2: define acronym PSD, power spectral density*

A: Defined as suggested.

T: (power spectral densities, PSD, vs frequency)

21. **Q:** *Page 12 line 6: "This picture is reminiscent of a GW-saturation process when vertical wavelength of GW becomes shorter." – could you provide a citation here?*

A: Reference provided as suggested.

T: (see, e.g., Fig. 5.3 in Nappo, 2002)

22. **Q:** *Page 12 paragraph 1: how does the wavelet spectrum shown in Fig. 12 for the down leg compare to that of the up leg?*

A: We noted in the text that the upleg spectra qualitatively agree, that is they show similar intermittent turbulence field.

T: We note that qualitatively similar picture in terms of turbulent structures could be inferred by analyzing the upleg data which is not shown here.

23. **Q:** *Page 12 line 9: are the O densities used here from the FIPEX instrument?*

A: We made it now clear in the text that the spectrum of neutral air density fluctuations is derived from the measurements by CONE instrument, whereas O-density fluctuations used to derive wavelet spectrum we obtained from the FIPEX measurements.

T: In Fig. 13 we further compare the neutral density spectrum derived from the CONE measurements with the spectrum of atomic oxygen density fluctuations derived from the FIPEX measurements.

24. **Q:** *Figure 13: would it be possible to highlight the altitudes of each 2D slice forming the three panels? These could also perhaps be shown in Fig. 12.*

A: By trying to address this reviewer's comment we realized that due to very high intermittency of the observed turbulence field, marking regions with different types of spectra makes figures extremely crowded and absolutely not readable. So, we decided to comment on it in the text.

T: Detailed analysis of all the regions where different types of O-density spectra occur is rather difficult because of different reasons. One reason is that when turbulence is very strong, its spectrum extends down to scales below current FIPEX resolution limit of $\sim$20 m, that is the O-density spectrum appears not fully resolved. So far we can only identify three regions where third type of spectra (like in Fig. 14c) was observed in the downleg measurements: between 90.9–91.2 km, 80.2–80.4 km, and 81.1–81.7 km.

25. **Q:** *Page 16 line 25: "usually attributed to GW" – could add a citation here*

A: We added the citation as suggested by the reviewer.

T: ...we see that they follow the k^{-3} slope, usually attributed to GW (see e.g., Smith et al., 1987; Weinstock, 1990; Fritts and Alexander, 2003; Žagar et al., 2017, and references therein),...

References

Arnold, K. S. and She, C. Y.: Metal fluorescence lidar (light detection and ranging) and the middle atmosphere, Contemporary Physics, 44, 35–49, https://doi.org/10.1080/00107510302713, 2003.

Asmus, H., Staszak, T., Strelnikov, B., Lübken, F.-J., Friedrich, M., and Rapp, M.: Estimate of size distribution of charged MSPs measured in situ in winter during the WADIS-2 sounding rocket campaign, Annales Geophysicae, 35, 979–998, https://doi.org/10.5194/angeo-35-979-2017, 2017.

Baumgarten, G.: Doppler Rayleigh/Mie/Raman lidar for wind and temperature measurements in the middle atmosphere up to 80 km, Atmospheric Measurement Techniques, 3, 1509, 2010.

Bishop, R. L., Larsen, M. F., Hecht, J. H., Liu, A. Z., and Gardner, C. S.: TOMEX: Mesospheric and lower thermospheric diffusivities and instability layers, Journal of Geophysical Research: Atmospheres, 109, https://doi.org/10.1029/2002JD003079, https://agupubs.onlinelibrary.wiley.com/doi/abs/10.1029/2002JD003079, 2004.

Eberhart, M., Löhle, S., Steinbeck, A., Binder, T., and Fasoulas, S.: Measurement of atomic oxygen in the middle atmosphere using solid electrolyte sensors and catalytic probes, Atmospheric Measurement Techniques, 8, 3701–3714, https://doi.org/10.5194/amt-8-3701-2015, 2015.

Eberhart, M., Löhle, S., Strelnikov, B., , Fasoulas, S., Lübken, F.-J., Rapp, M., Hedin, J., Khaplanov, M., and Gumbel, J.: Atomic oxygen number densities in the MLT region measured by solid electrolyte sensors on WADIS-2, Atmospheric Measurement Techniques, submitted, this issue, 2018.

Feofilov, A. G. and Kutepov, A. A.: Infrared Radiation in the Mesosphere and Lower Thermosphere: Energetic Effects and Remote Sensing, Surveys in Geophysics, 33, 1231–1280, https://doi.org/10.1007/s10712-012-9204-0, https://doi.org/10.1007/s10712-012-9204-0, 2012.

Fomichev, V. I., Ogibalov, V. P., and Beagley, S. R.: Solar heating by the near-IR CO2 bands in the mesosphere, Geophysical Research Letters, 31, https://doi.org/10.1029/2004GL020324, https://agupubs.onlinelibrary.wiley.com/doi/abs/10.1029/2004GL020324, 2004.

Friedrich, M.: Handbook of the Lower Ionosphere, Verlag der Technischen Universität Graz, https://doi.org/10.3217/ 978-3-85125-485-3, https://lampx.tugraz.at/~karl/verlagspdf/ionosphere_friedrich_ebook.pdf, 2016.

Friedrich, M. and Torkar, K.: High-latitude plasma densities and their relation to riometer absorption, Journal of Atmospheric and Terrestrial Physics, 45, 127 – 135, https://doi.org/https://doi.org/10.1016/S0021-9169(83)80017-8, http://www.sciencedirect.com/science/article/pii/S0021916983800178, 1983.

Fritts, D. C. and Alexander, M. J.: Gravity wave dynamics and effects in the middle atmosphere, Reviews of Geophysics, 41, 1003, https://doi.org/10.1029/2001RG000106, 2003.

Fukao, S., Yamanaka, M., Ao, N., K Hocking, W., Sato, T., Yamamoto, M., Nakamura, T., Tsuda, T., Kato, S., and , b.: Seasonal variability of vertical eddy diffusivity in the middle atmosphere 1. Three-year observations by the middle and upper atmosphere radar, Journal of Geophysical Research, 99, 18 973–18 987, https://doi.org/10.1029/94JD00911, 1994.

Gumbel, J.: Aerodynamic influences on atmospheric in situ measurements from sounding rockets, Journal of Geophysical Research: Space Physics, 106, 10 553–10 563, https://doi.org/10.1029/2000JA900166, https://agupubs.onlinelibrary.wiley.com/doi/abs/10.1029/2000JA900166, 2001.

Gumbel, J., Rapp, M., and Unckell, C.: Aerodynamic Aspects of Rocket-Borne in situ Studies, in: European Rocket and Balloon Programs and Related Research, edited by Kaldeich-Schürmann, B., vol. 437 of *ESA Special Publication*, p. 459, 1999.

Hauchecorne, A. and Chanin, M.-L.: Density and temperature profiles obtained by lidar between 35 and 70 km, Geophys. Res. Lett., 7, 565–568, https://doi.org/10.1029/GL007i008p00565, 1980.

Hedin, J., Gumbel, J., and Rapp, M.: On the efficiency of rocket-borne particle detection in the mesosphere, Atmospheric Chemistry and Physics, 7, 3701–3711, https://doi.org/10.5194/acp-7-3701-2007, https://www.atmos-chem-phys.net/7/3701/2007/, 2007.

Heisenberg, W.: Zur statistischen Theorie der Turbulenz, Z. Physik, 124, 628–657, 1948.

Höffner, J. and Fricke-Begemann, C.: Accurate lidar temperatures with narrowband filters, Opt. Lett., 30, 890–892, https://doi.org/10.1364/OL.30.000890, http://ol.osa.org/abstract.cfm?URI=ol-30-8-890, 2005.

Höffner, J. and Lautenbach, J.: Daylight measurements of mesopause temperature and vertical wind with the mobile scanning iron lidar, Opt. Lett., 34, 1351–1353, https://doi.org/10.1364/OL.34.001351, http://ol.osa.org/abstract.cfm?URI=ol-34-9-1351, 2009.

Latteck, R. and Bremer, J.: Long-term variations of polar mesospheric summer echoes observed at Andøya (69°N), Journal of Atmospheric and Solar-Terrestrial Physics, 163, 31 – 37, https://doi.org/https://doi.org/10.1016/j.jastp.2017.07.005, http://www.sciencedirect.com/science/article/pii/S1364682617300846, long-term changes and trends in the upper atmosphere, 2017.

Latteck, R. and Strelnikova, I.: Extended observations of polar mesosphere winter echoes over Andøya (69°N) using MAARSY, Journal of Geophysical Research (Atmospheres), 120, 8216–8226, https://doi.org/10.1002/2015JD023291, 2015.

Lautenbach, J. and Höffner, J.: Scanning iron temperature lidar for mesopause temperature observation, Appl. Opt., 43, 4559–4563, https://doi.org/10.1364/AO.43.004559, http://ao.osa.org/abstract.cfm?URI=ao-43-23-4559, 2004.

Lübken, F.-J.: On the extraction of turbulent parameters from atmospheric density fluctuations, J. Geophys. Res., 97, 20,385–20,395, 1992.

Lübken, F.-J.: Seasonal variation of turbulent energy dissipation rates at high latitudes as determined by insitu measurements of neutral density fluctuations, J. Geophys. Res., 102, 13,441–13,456, 1997.

Lübken, F.-J., Hillert, W., Lehmacher, G., and von Zahn, U.: Experiments revealing small impact of turbulence on the energy budget of the mesosphere and lower thermosphere, J. Geophys. Res., 98, 20,369–20,384, 1993.

Lübken, F.-J., Rapp, M., and Hoffmann, P.: Neutral air turbulence and temperatures in the vicinity of polar mesosphere summer echoes, J. Geophys. Res., 107(D15), 4273–4277, https://doi.org/10.1029/2001JD000 915, 2002.

Lübken, F.-J., Berger, U., and Baumgarten, G.: Temperature trends in the midlatitude summer mesosphere, Journal of Geophysical Research (Atmospheres), 118, 13, https://doi.org/10.1002/2013JD020576, 2013.

McKinnell, L.-A. and Friedrich, M.: A neural network-based ionospheric model for the auroral zone, Journal of Atmospheric and Solar-Terrestrial Physics, 69, 1459–1470, https://doi.org/10.1016/j.jastp.2007.05.003, 2007.

Mlynczak, M. G.: Energetics of the middle atmosphere: Theory and observation requirements, Adv. Space Res., 17(11), 117 – 126, 1996.

Nappo, C. J.: An introduction to atmospheric gravity waves, 2002.

Rapp, M., Gumbel, J., and Lübken, F.-J.: Absolute density measurements in the middle atmosphere, Ann. Geophys., 19, 571–580, 2001.

Selvaraj, D., Patra, A. K., and Narayana Rao, D.: On the seasonal variations of reflectivity and turbulence characteristics of low-latitude mesospheric echoes over Gadanki, Journal of Geophysical Research: Atmospheres, 121, 6164–6177, https://doi.org/10.1002/2015JD024283, https://agupubs.onlinelibrary.wiley.com/doi/abs/10.1002/2015JD024283.

She, C. Y., Vance, J. D., Williams, B. P., Krueger, D. A., Moosmüller, H., Gibson-Wilde, D., and Fritts, D.: Lidar studies of atmospheric dynamics near polar mesopause, Eos, Transactions American Geophysical Union, 83, 289–293, https://doi.org/10.1029/2002EO000206, https://agupubs.onlinelibrary.wiley.com/doi/abs/10.1029/2002EO000206.

Smith, S. A., Fritts, D. C., and Vanzandt, T. E.: Evidence for a Saturated Spectrum of Atmospheric Gravity Waves., Journal of Atmospheric Sciences, 44, 1404–1410, https://doi.org/10.1175/1520-0469(1987)044<1404:EFASSO>2.0.CO;2, 1987.

Staszak, T., Brede, M., and Strelnikov, B.: Open Source Software Openfoam as a New Aerodynamical Simulation Tool for Rocket-Borne Measurements, in: 22nd ESA Symposium on European Rocket and Balloon Programmes and Related Research, edited by Ouwehand, L., vol. 730 of *ESA Special Publication*, p. 201, 2015.

Strelnikov, B., Rapp, M., and Lübken, F.-J.: A new technique for the analysis of neutral air density fluctuations measured in situ in the middle atmosphere, Geophysical Research Letters, 30, 2052, https://doi.org/doi:10.1029/2003GL018271, 2003.

Strelnikov, B., Rapp, M., and Lübken, F.: In-situ density measurements in the mesosphere/lower thermosphere region with the TOTAL and CONE instruments, pp. 1–11, Terrapub, https://doi.org/10.5047/aisi.001, 2013.

Strelnikov, B., Szewczyk, A., Strelnikova, I., Latteck, R., Baumgarten, G., Lübken, F.-J., Rapp, M., Fasoulas, S., Löhle, S., Eberhart, M., Hoppe, U.-P., Dunker, T., Friedrich, M., Hedin, J., Khaplanov, M., Gumbel, J., and Barjatya, A.: Spatial and temporal variability in MLT turbulence inferred from in situ and ground-based observations during the WADIS-1 sounding rocket campaign, Annales Geophysicae, 35, 547–565, https://doi.org/10.5194/angeo-35-547-2017, 2017.

Szewczyk, A.: Mesospheric turbulence: The role in the creation of mesospheric inversion layers and statistical results, Ph.D. thesis, Universität Rostock, 2015.

Szewczyk, A., Strelnikov, B., Rapp, M., Strelnikova, I., Baumgarten, G., Kaifler, N., Dunker, T., and Hoppe, U.-P.: Simultaneous observations of a Mesospheric Inversion Layer and turbulence during the ECOMA-2010 rocket campaign, Ann. Geophys., 31, 775–785, https://doi.org/10.5194/angeo-31-775-2013, 2013.

Tatarskii, V. I.: The effects of the turbulent atmosphere on wave propagation, Jerusalem: Israel Program for Scientific Translations, 1971.

Žagar, N., Jelić, D., Blaauw, M., and Bechtold, P.: Energy Spectra and Inertia-Gravity Waves in Global Analyses, Journal of Atmospheric Sciences, 74, 2447–2466, https://doi.org/10.1175/JAS-D-16-0341.1, 2017.

von Zahn, U., von Cossart, G., Fiedler, J., Fricke, K. H., Nelke, G., Baumgarten, G., Rees, D., Hauchecorne, A., and Adolfsen, K.: The ALOMAR Rayleigh/Mie/Raman lidar: objectives, configuration, and performance, Ann. Geophys., 18, 815–833, https://doi.org/10.1007/s005850000210, 2000.

Weinstock, J.: Saturated and Unsaturated Spectra of Gravity Waves and Scale-Dependent Diffusion., Journal of Atmospheric Sciences, 47, 2211–2226, https://doi.org/10.1175/1520-0469(1990)047<2211:SAUSOG>2.0.CO;2, 1990.

Wörl, R., Strelnikov, B., Viehl, T. P., Höffner, J., Pautet, P.-D., Taylor, M. J., Zhao, Y., and Lübken, F.-J.: Thermal structure of the mesopause region during the WADIS-2 rocket campaign, Atmospheric Chemistry and Physics, 19, 77–88, https://doi.org/10.5194/acp-19-77-2019, https://www.atmos-chem-phys.net/19/77/2019/, 2019.

Yamada, Y., Fukunishi, H., Nakamura, T., and Tsuda, T.: Breaking of small-scale gravity wave and transition to turbulence observed in OH airglow, Geophysical Research Letters, 28, 2153–2156, https://doi.org/10.1029/2000GL011945, 2001.

Simultaneous ~~in situ~~ in-situ measurements of small-scale structures in neutral, plasma, and atomic oxygen densities during WADIS sounding rocket project

Boris Strelnikov[1], Martin Eberhart[4], Martin Friedrich[5], Jonas Hedin[3], Mikhail Khaplanov[3†], Gerd Baumgarten[1], Bifford P. Williams[6], Tristan Staszak[1], Heiner Asmus[1], Irina Strelnikova[1], Ralph Latteck[1], Mykhaylo Grygalashvyly[1], Franz-Josef Lübken[1], Josef Höffner[1], Raimund Wörl[1], Jörg Gumbel[3], Stefan Löhle[4], Stefanos Fasoulas[4], Markus Rapp[2], Aroh Barjatya[7], Michael J. Taylor[8], and Pierre-Dominique Pautet[8]

[1]Leibniz-Institute of Atmospheric Physics at the Rostock University, Kühlungsborn, Germany
[2]Deutsches Zentrum für Luft- und Raumfahrt, Institut für Physik der Atmosphäre, Oberpfaffenhofen, Germany
[3]Department of Meteorology (MISU), Stockholm University, Stockholm, Sweden
[4]University of Stuttgart, Institute of Space Systems, Stuttgart, Germany
[5]Graz University of Technology, Graz, Austria
[6]GATS, Boulder, USA
[7]Embry-Riddle Aeronautical University, FL, USA
[8]Center for Atmospheric and Space Sciences, Utah State University, Logan, Utah, USA
[†]Deceased

Correspondence: B. Strelnikov (strelnikov@iap-kborn.de)

Abstract. In this paper we present an overview of measurements conducted during the WADIS-2 rocket campaign. We investigate the effect of small-scale processes like gravity waves and turbulence on the distribution of atomic oxygen and other species in the MLT region. Our analysis suggests that density fluctuations of atomic oxygen are coupled to fluctuations of other constituents, i.e., plasma and neutrals. Our measurements show that all measured quantities, including winds, densities, and temperatures, reveal signatures of both waves and turbulence. We show observations of gravity wave saturation and breakdown together with simultaneous measurements of generated turbulence. Atomic oxygen inside turbulence layers shows two different spectral behaviors, which might imply change of its diffusion properties.

1 Introduction

The mesosphere, lower thermosphere (MLT) region is host of phenomena that are connected to dynamic and chemical processes which are still not fully understood. Thus, e.g., it is generally accepted that atmospheric gravity waves (GW) play an essential role in the dynamics of this region and that they couple it with the lower and upper atmosphere (e.g., Becker and Schmitz, 2002; Fritts and Alexander, 2003; Alexander et al., 2010). When propagating, GW might dissipate and thereby generate turbulence (e.g., Yamada et al., 2001; Selvaraj et al., and references therein). Apart of the momentum deposition, which is a key coupling process, this also affects mixing and redistribution of trace constituents (e.g., Fukao et al., 1994; Bishop et al., 2004) . One of the most important trace constituents in MLT is atomic oxygen (O) which plays an essential role in the chemistry and

energy budget of the mesopause region (e.g., Mlynczak and Solomon, 1993). It is the major reactive trace constituent in the mesosphere/lower thermosphere (MLT) region and it plays a crucial role in different chemical reactions involved in airglow excitation or ion chemistry (e.g., Walterscheid et al., 1987; McDade et al., 1986; McDade, 1998; Marsh et al., 2006; Caridade et al., 2013; Lednyts'kyy et al., 2015). The lifetime of atomic oxygen varies with altitude from seconds at ∼50 km to months at ∼100 km (e.g., Torr, 1985; Smith et al., 2010).

Chemical heat released during exothermic reactions involving atomic oxygen is one of the main contributors to the energy budget of this region (e.g., Mlynczak and Solomon, 1991; Mlynczak and Solomon, 1993). These reactions yield chemical heating rates in the mesopause region of several K/day which is comparable (or even competitive) to those of turbulent heating (Lübken, 1997; Lübken et al., 2002) as well as direct heating due to solar radiation (e.g., Fomichev et al., 2004; Feofilov and Kutepov, 2012 . Oxygen is involved in exothermic reactions with hydroxyl (OH) which emission bands have been extensively used to study the mesopause-region temperature, gravity waves, and tides (e.g., Hines and Tarasick, 1987; Taylor et al., 1995, 1997, 2009; Snively, 2013; Fritts et al., 2014; Egito et al., 2017, and references therein).

It is believed that at altitudes where the O-lifetime is very long, i.e., roughly above 90 km, variations in O-density ~~manly~~ mainly result from dynamical processes such as GW, tides, and the large scale circulation. Whereas at lower heights chemical processes may play a crucial role in forming O-density variations. It is also known, that mesopause region is very active dynamically. It is region where GW break and a persistent turbulence field plays crucial role in global circulation (e.g., Becker and Schmitz, 2002; Fritts and Alexander, 2003; Rapp et al., 2004). However, it is not known, for instance, how turbulence influences the O-density distribution, its diffusion properties and whether it can affects chemical heat release e.g., by changing reaction rates.

This implies that in order to properly characterize the chemical and dynamical state of the mesopause region, it is important to know the altitude resolved concentration of atomic oxygen alongside with the state of the background atmosphere including its thermal structure and dynamical parameters.

All these aspects stress the importance of common-volume measurements of the oxygen density together with temperature and density of the background neutral atmosphere with a sufficiently high altitude resolution.

This paper aims at two things. First, it is to provide an overview of the WADIS-2 sounding rocket campaign and measured parameters, and second, to ~~study the effect of~~ demonstrate that gravity wave motions and turbulence ~~on the~~ effects distribution of atomic oxygen in the nighttime MLT region. We present results of ~~in situ~~ in-situ and some ground based measurements obtained in the frame of the WADIS sounding rocket mission. We introduce new high resolution O-density measurements in connection with other parameters of the atmosphere. The paper is structured as follows. In Sec. 2 we briefly describe the WADIS-2 mission and measurement techniques used in this study. In Sec. 3 we present measurement results followed by a more detailed analysis in Sec. 4. In Sec. 5 we critically discuss ~~the~~ our findings and finally, in Sec. 6 we summarize main results and give an outlook to our next rocket borne measurements.

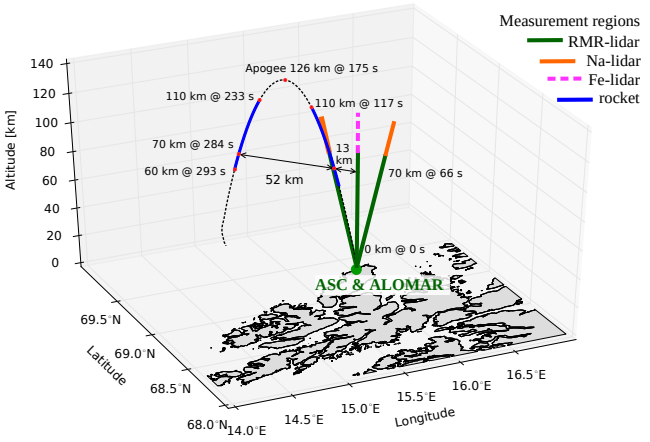

Figure 1. Schematics of WADIS-2 rocket experiment. Solid green and orange, and dashed magenta lines show ALOMAR RMR-, Na-, and IAP Fe-lidar measurement volumes, respectively. Black dashed line shows rocket trajectory. Blue lines show rocket measurement range used in this study.

2 WADIS-2 rocket campaign and instrumentation

The WADIS sounding rocket mission led by the Leibniz-Institute of Atmospheric Physics (IAP) in Kühlungsborn, Germany, in partnership with the Institute of Space Systems (IRS) in Stuttgart and contributions from Austria, Sweden, the USA, and Norway, comprised two field campaigns conducted at the Andøya Space Center (ACS) in northern Norway (69°N, 16°E). The first campaign was conducted in June 2013 and the second in March 2015. WADIS stands for "Wave propagation and dissipation in the middle atmosphere: Energy budget and distribution of trace constituents". The mission aimed at studying the propagation and dissipation of gravity waves (GW) and measuring concentration of atomic oxygen simultaneously. Such measurements allow for estimation of the contribution of chemical and turbulent heating to the energy budget of the MLT, as well as the transport of atomic oxygen by waves and turbulence. For a more detailed mission description the reader is referred to Strelnikov et al. (2017). The Arctic Lidar Observatory for Middle Atmosphere Research (ALOMAR, von Zahn et al., 1995) is located close the launch site and was an integral part of the entire WADIS mission.

The launch window for the second sounding rocket campaign was scheduled around local midnight to ensure full night-time conditions. A large number of ground-based optical instruments were supporting the WADIS-2 rocket campaign. The ALOMAR ~~RMR-~~Rayleigh/Mie/Raman (RMR)-, Na Weber, and IAP Fe-lidar were running continuously throughout the campaign period whenever weather permitted. ~~Also the~~ All three lidars measure temperatures profiles along the beam direction as shown in Fig. 1. The instruments and temperature retrieval techniques for these lidars are described elsewhere (von Zahn et al., 2000; Hauchecorne . Additionally, RMR- and Na-lidars measure line-of-sight wind speed in the altitude ranges 20–80 and 80–110 km, respectively (Baumgarten, 2010; Arnold and She, 2003).

The Advanced Mesospheric Temperature Mapper (AMTM) by Utah State University (Pautet et al., 2014) was observing the night glow emissions at 1523.68 and 1542.79 nm. These observations yield measurements of horizontal temperature field (see Fig. 4 and Wörl et al., 2019, for a detailed discussion of measurements during WADIS-2 campaign).

The Middle Atmosphere ALOMAR Radar System, MAARSY, (Rapp et al., 2011; Latteck et al., 2012) operated by IAP located close to the rocket launch site was continuously running. MAARSY was used to detect polar mesospheric winter echoes (PMWE) in case ~~they should~~ if they occur (Latteck and Strelnikova, 2015).

The instrumented WADIS-2 payload was almost identical to that one launched during the first campaign (see Strelnikov et al., 2017, for details), except that the instruments were tuned for the polar night launch conditions.

The front and rear decks of the WADIS payloads were equipped with identical CONE ionization gauges to measure turbulence, neutral air density, and temperature on up- and downleg (Strelnikov et al., 2013). CONE measures density of neutral air with altitude resolution of $\sim$30 cm. Making use of laboratory calibrations allows to derive absolute density altitude-profile. The measured density profile, in turn, can be integrated assuming hydrostatic equilibrium to yield temperature profile (see e.g., Strelnikov et al., . High sensitivity of the CONE instrument, which allows to resolve density fluctuations of $\sim$0.01 %, makes it possible to derive turbulent parameters by analyzing the spectra of these fluctuations. The derivation technique of turbulent parameters is described in detail elsewhere Lübken (1992); Lübken et al. (1993); Lübken (1997); Strelnikov et al. (2003); Strelnikov et al. (2013) . Briefly, a theoretical spectral model of turbulence is fitted to a Fourier or wavelet spectrum of the measured relative density fluctuations, which are shown to be a conservative and passive turbulence tracer in MLT (Lübken, 1992; Lübken et al., 1993; Lübken, 1997) . The key-feature of this technique is that the theoretical model must reproduce spectrum of turbulent tracer (scalar) in both inertial (i.e. $\propto k^{-5/3}$) and viscous (or dissipation) subranges. Transition between these subranges takes place at the so called inner scale, l_0, which is related to the turbulence energy dissipation rate, ε as $l_0 = C(\nu^3/\varepsilon)^{(1/4)}$, where ν is the kinematic viscosity and the constant C is of the order 10. Also, Lübken et al. (1993) and Lübken (1997) showed that different spectral models, in particular those by Heisenberg (1948) and by Tatarskii (1971), yield close results of the energy dissipation rates.

A positive ion probe (PIP) operated by the University of Technology in Graz (TUG), Austria, and novel Langmuir probe (LP) developed and operated by Embry-Riddle Aeronautical University in Florida, USA, yielded high-resolution positive ion and electron density measurement, respectively. Both these plasma probes were mounted on booms located on the rear deck of the payload.

Two instruments, the FIPEX and an airglow photometer, were used to measure atomic oxygen densities. These instruments, utilized entirely different measurement techniques. Photometers yield precise absolute density measurements, whereas FIPEX yields high altitude resolution data. The absolute values of the FIPEX-measurements were validated by the Photometers ~~(see Eberhart et al., 2018, for more details)~~(see companion paper by Eberhart et al., 2018, for more details).

The FIPEX instruments developed by IRS, yield profiles of atomic oxygen densities with high altitude resolution of $\sim$20 m (see Eberhart et al., 2015). Photometers operated by the Meteorological Institute at Stockholm University (MISU) measured oxygen densities using a well established reliable technique applied before on a large number of sounding rockets (e.g., Hedin et al., 2009).

FIPEX stands for „Flux-Probe-Experiment“, it employs solid electrolyte sensors having gold electrodes with selective sensitivity towards atomic oxygen. A low voltage is applied between anode and cathode pumping oxygen ions through the electrolyte ceramic (yttria stabilized zirconia, YSZ). The current measured is proportional to the oxygen flux. A detailed description of measurements conducted by FIPEX during WADIS mission is provided by Eberhart et al. (2015) and Eberhart et al. (2018) for the first and second campaign, respectively.

The MISU airglow photometer measures emission of the molecular oxygen Atmospheric Band around 762 nm from the overhead column, from which volume emission rate is inferred by differentiation. A theory and application of oxygen density retrievals from the Atmospheric Band emissions is discussed in details in the companion paper by Grygalashvyly et al. (2019) .

The second MISU photometer on the payload measured the emission from the (0-0) band of the N_2^+ 1st negative band system centered at 391.4 nm. This emission is a sign of precipitating auroral electrons and thus a sensitive indicator of auroral activity.

The WADIS-2 sounding rocket was launched on 5th of March 2015 at 01:44:00 UTC, that is during full night-time conditions. Fig. 1 shows the geometry of the WADIS-2 experiment. The black dashed parabola shows the actual rocket trajectory. The blue profiles show parts of the rocket trajectory which yielded measurements used in this paper. The solid green, orange, and dashed magenta lines show direction and altitude range for RMR-, Na, and Fe-lidar, respectively. It is seen, that the north-west (NW) directed lidar beam was co-located with the ascending part of the rocket trajectory.

3 Data

In this section we show data obtained by ground-based instruments around the rocket launch time and some profiles measured on board the WADIS-2 sounding rocket. We start with measurements of the background state of the atmosphere as observed during the night of the rocket launch. Then we compare upleg and downleg density measurements conducted by different instruments. These profiles are then used in Sec. 4 for a detailed fluctuation analysis. Finally, we demonstrate that the high-resolution FIPEX-measurements yielded new, geophysically meaningful data.

3.1 Background

The background state of the atmosphere was continuously monitored by the ALOMAR lidars and radars. MAARSY did not observe any echoes during the night of the rocket launch. That is, the WADIS-2 rocket launch was under conditions of confirmed absence of polar mesospheric winter echoes, PMWE. Fig. 2 shows volume reflectivity measured by MAARSY during 5 of March, i.e. the day of the rocket launch. Some short-living echoes were observed around noon and in the late evening, but not in the morning when WADIS-2 rocket was launched. We recall here that this sounding rocket mission did not aim at studying PMWE, so that the presence of PMWE was not a criterion for rocket launch.

Thanks to favorable weather conditions, the lidars were able to measure both temperature and wind fields for several hours around rocket launch time.

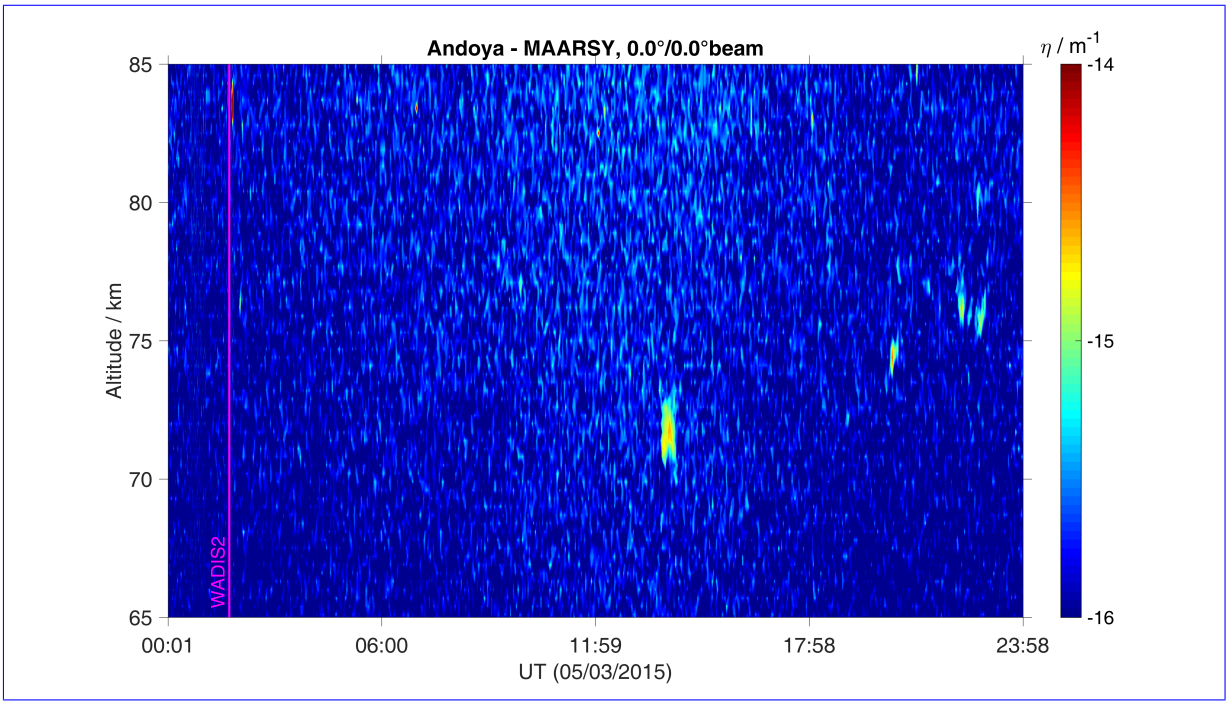

Figure 2. ~~Combined RMR-~~ Volume reflectivity measured by MAARSY on 5 of March. Some short-living echoes were observed around noon and ~~Fe-lidar temperature measurements during~~ in the ~~night of~~ late evening but not around the WADIS-2 rocket launch~~, i. e. 4 to 5 of March 2015.~~

Fig. 3 shows the temperature field measured by the IAP RMR- and Fe-lidars from 20 up to ∼100 km altitude around the time of the WADIS-2 rocket launch. Fig. 3 utilizes measurements by the vertical beam of RMR-lidar since the mobile Fe-lidar only measures vertically. Also, the seeding temperature for derivation of RMR-temperatures was taken from Fe-lidar measurements. Signatures of long period waves are clearly seen above ∼65 km altitude ~~,~~ in both RMR- and Fe-lidar measurements.

Horizontal temperature field observed by the AMTM (Pautet et al., 2014) shown in Fig. 4 also reveals clear large scale structures around the WADIS-2 launch time. Wörl et al. (2019) analyzed the co-located temperature measurements by both Fe-lidar and AMTM in detail and concluded that the most pronounced wave signatures reveal periods of 24, 12, and 8 hours i.e., they are most probably created by tides.

Fig. 5 shows measurements by the Na-lidar conducted throughout the night of the WADIS-2 launch. Similar to Fe-temperature these measurements show prominent signatures of long period waves above 80 km altitude in both temperature and wind fields.

All these data contain also smaller scale fluctuations which result from gravity waves and turbulence. To see such small-scale fluctuations better and analyze them properly, one has to subtract the large-scale background (including tides) from the measurements shown in Fig. 3, 4, and 5 ~~(see e.g., ?)~~(see e.g., Strelnikova et al., 2019). In the next section we focus on small-scale fluctuations of different quantities. We analyze rocket-borne instant measurements and further compare these with profiles measured by the ground-based instruments at the time of rocket launch.

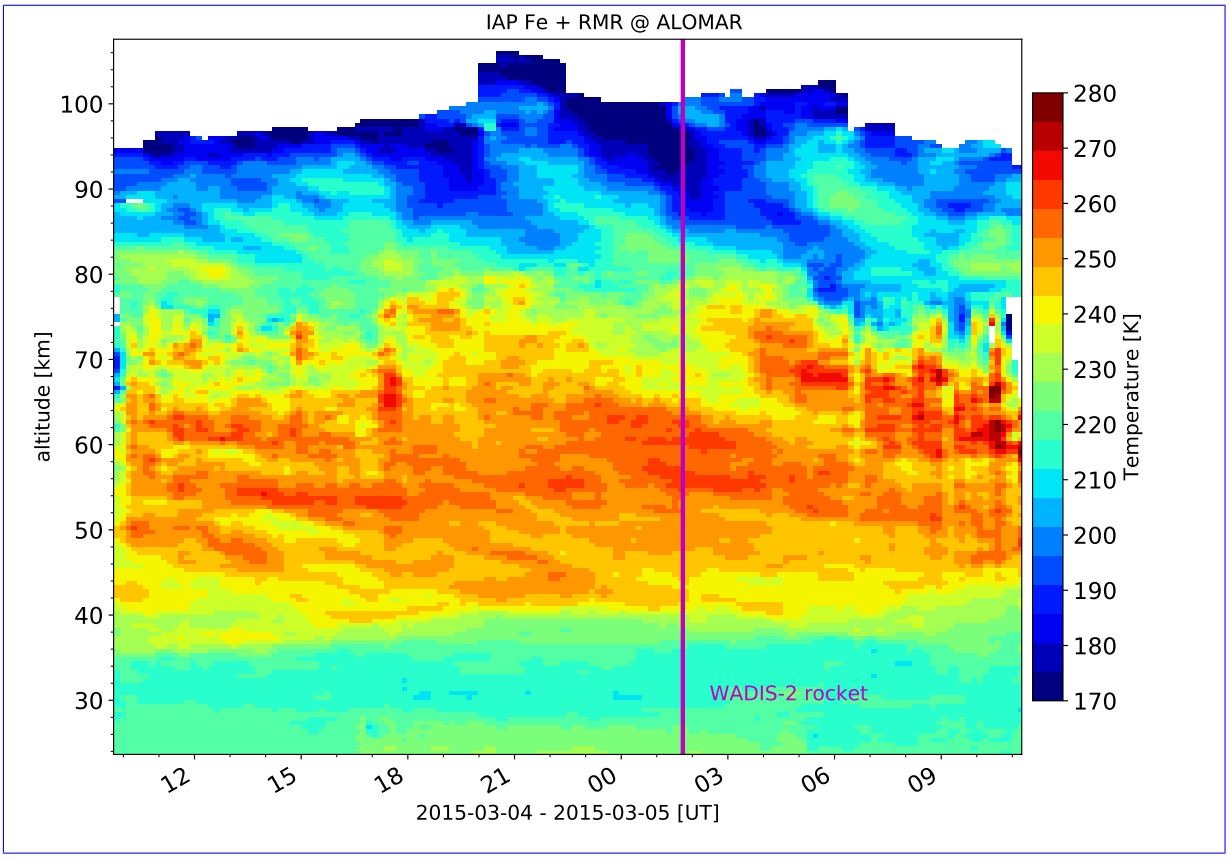

Figure 3. Combined RMR- and Fe-lidar temperature measurements during the night of the WADIS-2 rocket launch, i.e. 4 to 5 of March 2015.

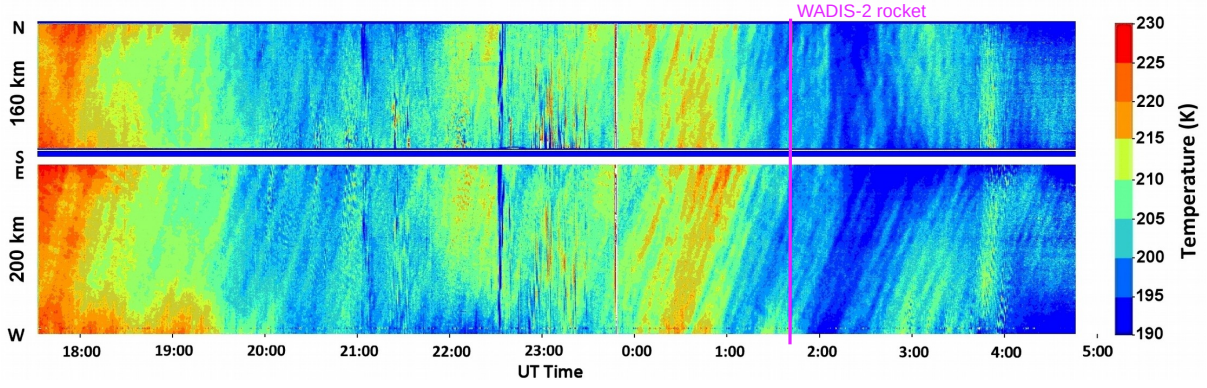

Figure 4. NS and WE keogram summary of the AMTM temperature measurements obtained during the night of 4 to 5 March 2015.

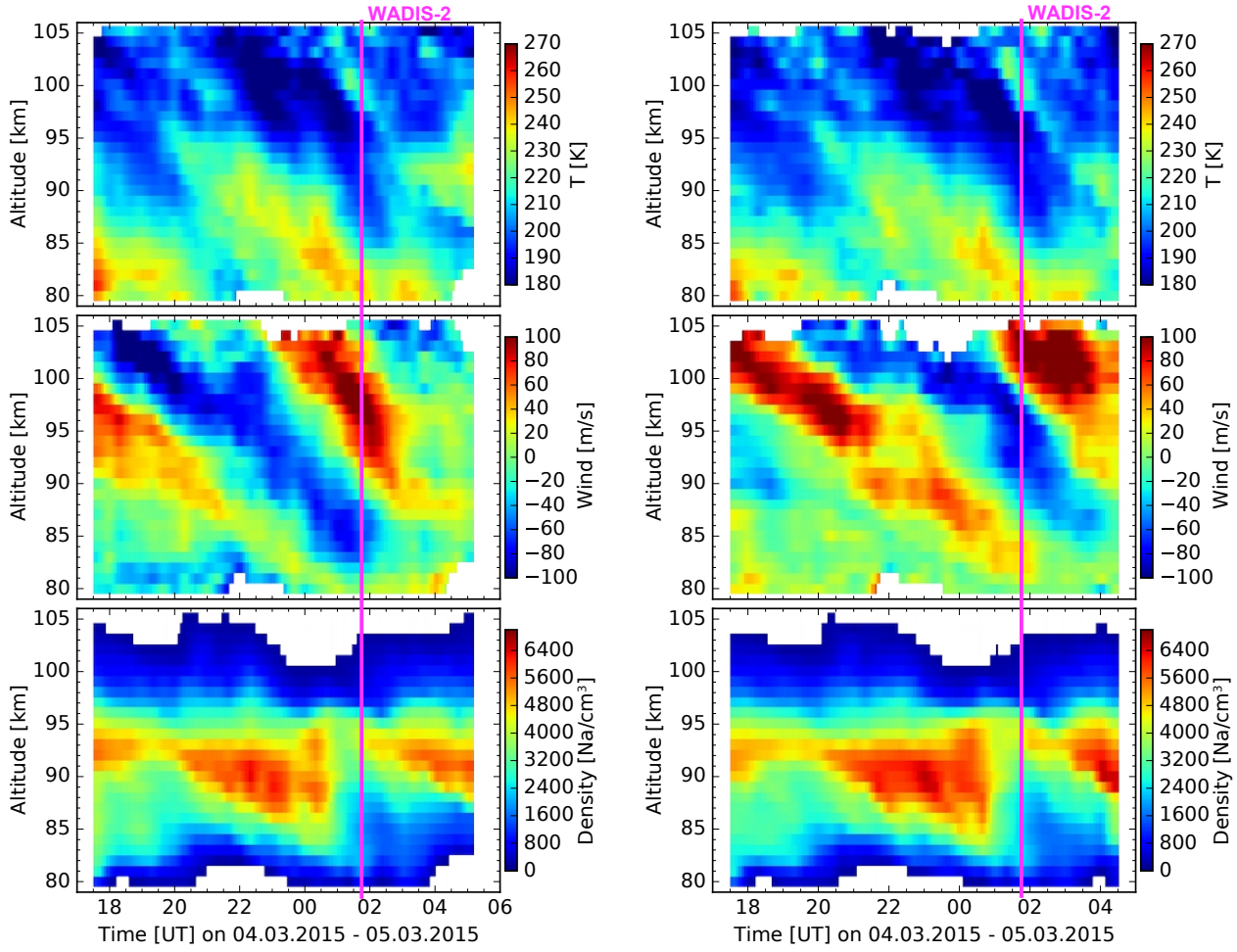

(a) North-West beam, i.e. close to rocket trajectory.

(b) South-East beam.

Figure 5. Na-lidar measurements during the night of the WADIS-2 rocket launch, i.e. 4 to 5 of March 2015. Rocket was launched at 1:44 UT

3.2 In-situ measurements

The WADIS-2 rocket was launched at 1:44 UTC and reached an apogee of 126 km. The measurement phase started at about 60 km altitude after nose-cone and motor separation. However the best quality data was obtained above 70 km height, mostly due to favorable aerodynamic conditions.

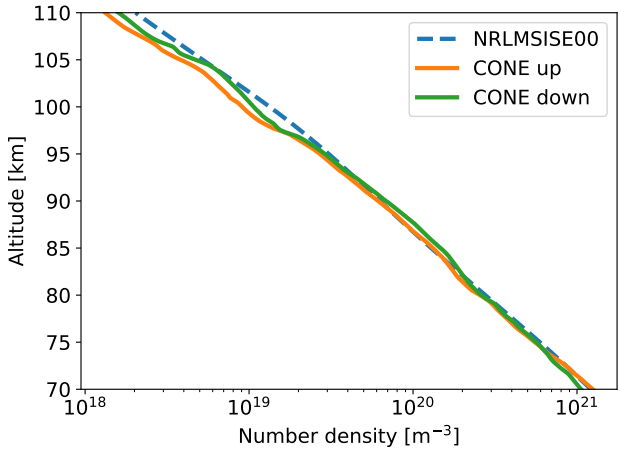

Figure 6. Rocket-borne density measurements by the ionization gauge CONE for upleg and downleg (orange and green lines, respectively). Blue dashed line shows the NRL-MSISE00 climatology for the time of WADIS-2 launch, i.e. 5 of March 2015, 01:44:00 UTC.

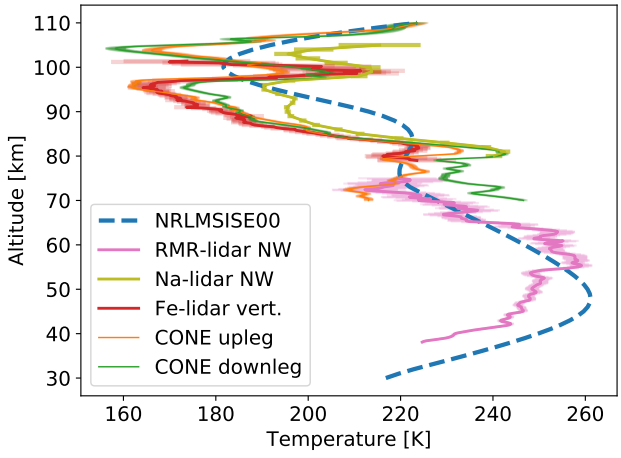

Figure 7. Temperatures derived from the densities shown in Fig. 6 assuming hydrostatic equilibrium: orange and green for upleg and downleg, respectively. Profiles in magenta, yellow, and red show measurements by RMR-, Na-, and Fe-lidars, respectively. Blue dashed line shows NRLMSISE-00 reference atmosphere for the time of WADIS-2 launch (5 of March 2015, 01:44:00 UTC).

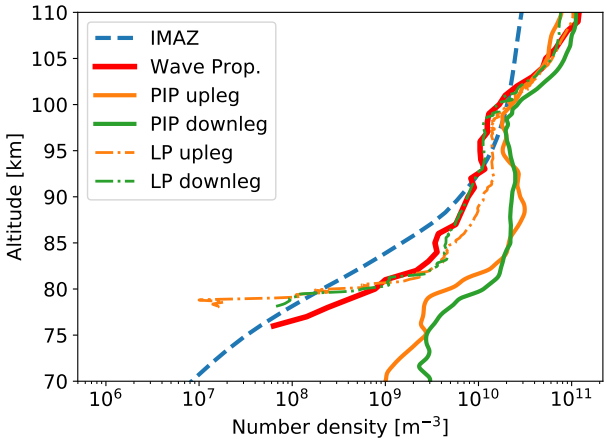

Figure 8. ~~Same as Fig. 6 but for~~ Densities of positive ion (solid orange and green lines) and electron (dash-dotted orange and green profiles) densities measured by the PIP and LP instruments, respectively. Bold solid red line shows results of the wave propagation experiment. Blue dashed line shows electron density from the empirical ionospheric model for the auroral zone, IMAZ, derived for the time of the WADIS-2 flight (see text for details).

Figs. 6 and 7 show ~~in situ measured~~ profiles of neutral air densities and temperatures measured in-situ by the CONE instrument. Orange and green lines show up- and downleg measurements, respectively. Blue dashed profiles represent NRLMSISE-00 reference atmosphere (Picone et al., 2002). The spin frequency of WADIS-2 rocket of 3.27 Hz which modulated the raw data was filtered out by applying a notch filter. Additionally, the shown in-situ measured densities were smoothed by running average of a length of ∼200 m.

Both up- and downleg profiles look very similar in terms of mean values and oscillations. The background atmosphere reveals a typical winter state (see e.g., Strelnikov et al., 2013, where a collection of rocket-borne measurements for different seasons is shown). Also, the observed turbulence activity shown in Sec. 4 demonstrates a typical for winter behavior. The temperature profiles clearly show some GW-signatures with amplitudes of up to 15 K at altitudes below 80 km. The height range between ∼83 and 90 km reveals very low GW amplitudes~~.~~, i.e. temperature fluctuations of 1 K and less. A temperature increase of ∼40 K reminiscent of mesospheric inversion layers (MIL) similar to those analyzed by Szewczyk et al. (2013) is seen between 95 and 100 km and is discussed in Sec. 4. Some small-scale GWs with amplitudes between 1 and 5 K and vertical wavelength of the order kilometer are superposed on this large temperature disturbance. Fig. 7 additionally shows temperature profiles in magenta, yellow, and red measured by RMR-, Na-, and Fe-lidars, respectively.

The neutral density profiles in Fig. 6 also show some oscillations that can be attributed to gravity waves, which will be analyzed in detail in Sec. 4.

In Fig. 8 we show profiles of electron and positive ion densities measured in-situ on both up- and downleg. Dashed-dotted and solid profiles show electron and positive ion data, respectively. The bold solid red line shows measurements results of the

wave propagation experiment. The two ion density profiles are also quite similar and also reveal some wave signatures. The two electron density profiles also demonstrate that ionospheric background at the rocket up- and downleg is rather similar. Comparison with ~~an~~ the electron density profile from the empirical ionospheric model for the auroral zone, IMAZ (McKinnell and Friedrich, 2007) shown in Fig. 8 (blue dashed line) shows that ionization level of the ionosphere was moderately high. This is in accord with the fact that some aurora was seen throughout the night of these observations. ~~Also, the auroral emission detector operated together with the airglow photometer by MISU registered some auroral emissions above 100 km height. The shown plasma density profiles yield relative density measurements and therefore, they were normalized to~~ The inputs for IMAZ model are F10.7 solar flux index of 137.9 Jy (1 Jy = 10^{-26} W m^{-2}Hz^{-1}), the planetary magnetic Ap index 5, and riometer absorption @ 27.6 MHz of 0.076 dB. Activity indices, the solar F10.7 and Ap index, were obtained from the GSFC/SPDF OMNIWeb interface at https://omniweb.gsfc.nasa.gov. The integral riometer absorption was estimated from the electron density measurements by wave propagation experiment based on Friedrich and Torkar (1983).

The overhead emission seen by the second MISU photometer was varying (both increasing and decreasing at times) during the flight indicating that the auroral emission was variable in time. The auroral emission was relatively weak with peak total band radiances of 700–800 Rayleighs (around $6 \cdot 10^7$ photon $\cdot$ s^{-1} str^{-1} cm^{-2}).

The PIP and LP instruments yield measurements of relative densities of positive ions and electrons, respectively. The wave propagation experiment ~~values at altitudes~~ yields accurate measurements of absolute electron densities, which are used to normalize the PIP- and LP-measurements. The normalization was made at an altitude of ∼115 km, where quasi-neutrality condition is well satisfied for ionospheric plasma (see e.g., Friedrich, 2016; Asmus et al., 2017, for more details). The large difference between positive ion and electron densities at altitudes ∼80–95 km was studied in detail by Asmus et al. (2017) and was shown to be due to charged dust particles.

Fig. 9 shows atomic oxygen density profiles measured by the photometer on up- and downleg in orange and green, respectively. The FIPEX measurements are only shown for the descending part of the WADIS-2 rocket flight, because we are mostly confident in their absolute values and will use this data for further analysis. The blue dashed line shows NRLMSIS-00 data and black dotted line shows SABER retrievals (orbit 71729, event 20) at ∼230 km distant location and ∼4 h before rocket launch. That is, the SABER measurements were not collocated and not simultaneous with the rocket flight and are only shown for qualitative comparison. However, the apparent density increase in SABER data above 100 km must rather be attributed to the observed auroral activity. We recall that the measurement principle of the FIPEX instrument is only sensitive to ambient O-density and does not react on emissions.

~~It is~~ We note here that the FIPEX is a new instrument which was first applied for oxygen density measurements on sounding rockets during WADIS-1 rocket campaign (Eberhart et al., 2015). It showed good results and demonstrated principal possibility of a high resolution O-density measurements in MLT. WADIS-2 rocket was additionally equipped with the MISU airglow photometer that indirectly measures O-density from emission of the molecular oxygen Atmospheric Band. Such type of measurements is widely used also from the ground- or satellite-based platforms and is commonly accepted as reliable. The WADIS-2 sounding rocket comprised the both measurement techniques on the same platform which made it possible to closely compare their results. The both WADIS payloads (i.e. for the first and second campaigns) were equipped with several

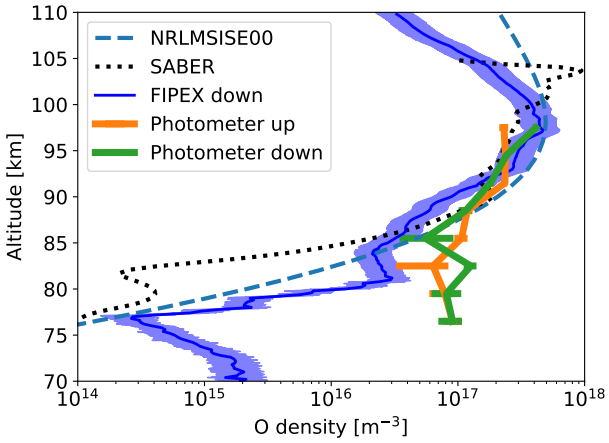

Figure 9. ~~Same as Fig. 6 but for atomic~~ Atomic oxygen densities ~~measured by photometers~~measurements. ~~Additionally~~Bold orange and green lines with error-bars show photometer measurements on up- and downleg, respectively. FIPEX downleg data is shown by blue profile with shaded area showing measurement errors~~and black~~. Black dotted line shows SABER measurements (Level 2A, O event 20 orbit 71729). Blue dashed line shows NRLMSISE-00 model data for the time of rocket launch.

FIPEX sensors which were mounted at different angles relative to rocket velocity (or rocket symmetry) axis. Such multiple configuration aimed at finding the most favorable aerodynamic orientation for the FIPEX sensors. We also note that because of the supersonic rocket velocity the measurement results of most instruments on board sounding rockets require an aerodynamic correction (Gumbel et al., 1999; Gumbel, 2001; Rapp et al., 2001; Hedin et al., 2007; Staszak et al., 2015). By analyzing measurement conditions and comparing the measurement results we chose the best quality FIPEX data for further analysis. For the detailed discussion of all FIPEX measurements the reader is referred to the companion paper by Eberhart et al. (2018).

It is already seen in Fig. 9 that the O-density profiles reveal some oscillations with largest amplitudes below approx. 83 km altitude. It is worth mentioning, that other FIPEX sensors yielded fluctuations data that show the same features (not shown here and discussed in detail in Eberhart et al., 2018)

The photometer measurements have an effective altitude resolution of 3 km, whereas the catalytic FIPEX sensors exhibit height resolution of $\sim$20 m. In the next section we examine which advantages the high resolution measurements of the atomic oxygen densities can bring and what the nature of the fluctuations in the FIPEX data is.

4 Analysis

To extract small-scale fluctuations from the measured profiles, we subtract the mean background derived as running average over 5 km long vertical window. Similar results can be achieved by e.g., applying a polynomial fit of the same vertical resolution, i.e. 5 km or by means of other techniques ~~(e.g., ?)~~(e.g., Strelnikova et al., 2019). We here focus on small vertical length scales $<$5 km comprising both turbulent fluctuations as well as part of the gravity wave spectrum. We note that choosing a

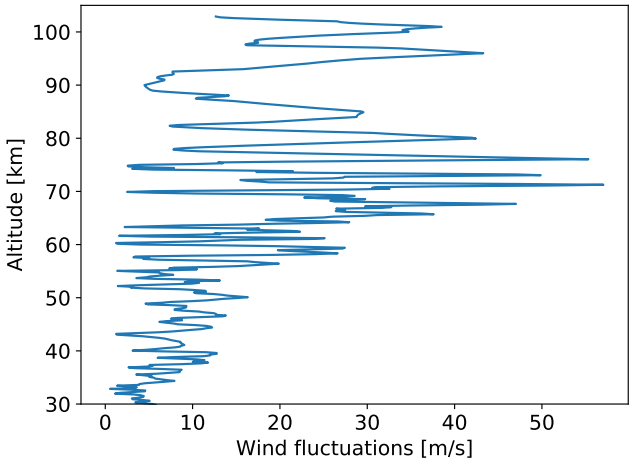

Figure 10. Horizontal wind fluctuations (i.e., $\sqrt{u'^2 + v'^2}$, where u' and v' are zonal and meridional wind fluctuations) derived from combined RMR- and Na-lidar measurements for the time of WADIS-2 rocket flight.

particular cut off wavelength always carries some degree of arbitrariness. For the small-scale ~~stuff~~ structures in MLT and, especially ~~turbulent structures~~those produced by turbulence, the background derivation does not affect the data analysis if residual fluctuations data contain all the scales below this limit (i.e. ∼5 km).

Fluctuations of horizontal wind derived from the lidar measurements for the time of the WADIS-2 rocket launch are shown in Fig. 10. It reveals an amplitude increase with height, z, according to the exponential law ($\propto$ exp(z/2H), where H is scale height). It demonstrates basically, that we observed gravity waves in the entire altitude range from near the ground up to ∼105 km. Wind fluctuation amplitude increases in the altitude range from 30 up to ∼70 km. Then the amplitude drops within altitude range 70 to 80 km and increases again between 88 and 95 km. This is consistent with the behavior of temperature profiles that show larger wave amplitudes below 80 km altitude, very low amplitudes above that height and large wave amplitude again between 95 and 105 km (Figs. 5 and 7).

In Fig. 11 we show relative density fluctuations (residuals) for neutrals, positive ions, and atomic oxygen in blue, orange, and green, respectively. These fluctuations were derived from the density profiles measured on the downleg of WADIS-2 rocket flight. All three profiles show wave-like oscillations with (vertical) wavelengths in the range 1 to 5 km that can be attributed to gravity waves. Between 103 and 110 km altitude all three profiles oscillate in phase. Below ∼103 km height these density fluctuations reveal similar wavelengths but shifted in phase relative to each other.

The density fluctuations of neutral gas shown in blue are used to derive turbulence energy dissipation rates, ε, as mentioned in Sec. 2. The resultant ε-profiles for up- and downleg are shown in Figs. 12a and 12b, respectively.

Blue and green profiles represent turbulence derivation utilizing different spectral models, i.e. of Heisenberg (1948) and Tatarskii (1971), respectively (see also e.g., Lübken et al., 1993). The difference between the green and the blue values can be considered as method's uncertainty. The black bold and grey profiles show climatologies, that is mean seasonal values

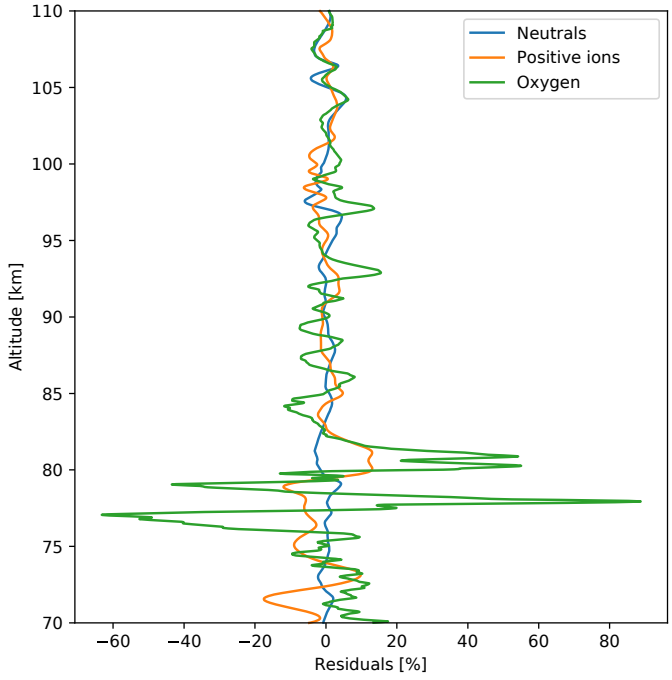

Figure 11. Relative density fluctuations (=residuals) of neutral air, positive ions, and atomic oxygen shown by blue, orange, and green profiles, respectively. These fluctuations were derived from the density profiles measured on the downleg of WADIS-2 rocket flight by subtracting a running average over 5 km long vertical window.

for winter ~~and summer~~(Lübken, 1997) and summer (Lübken et al., 2002), respectively. Fig. 12 reveals, for instance, that we observed turbulence activity in the entire altitude range from 60 up to 100 km. This is a characteristic feature for winter season. Also the upleg and downleg turbulence data qualitatively agree with each other except small region observed between 63 and 67 km on downleg. Vertical thick lines in Fig. 12 show mean values over the marked altitude regions (i.e., 10 km altitude bins). If compared with results of our previous rocket campaign WADIS-1 that was conducted in summer (Strelnikov et al., 2017), the observed winter turbulence field does not show big difference between up- and downleg measurements. If taking only mean values with their uncertainties in consideration, the height region 70 to 100 km looks very similar on both up- and downleg. The downleg turbulence measurements, however, reveal a patch of very strong turbulence around ∼65 km height. Turbulence filed in summer MLT observed during WADIS-1 campaign showed large oscillations in both space and time so that even mean ε-values of up- and downleg rocket measurements differed by order of magnitude (Strelnikov et al., 2017). Turbulence variability in time was studied by analyzing MAARSY and EISCAT (European Incoherent SCATter Scientific Association) radar measurements which were properly scaled based on in-situ data. The MAARSY is only capable of measuring MLT parameters if some radar echo occurs, that is it needs presence of PMSE or PMWE. PMSE occurrence rate as observed by MAARSY is close to 100 % (Latteck and Bremer, 2017) which makes it easy to study MLT in summer season. The winter echoes, PMWE, are much more rare, i.e. their occurrence rate is at most 30 % (Latteck and Strelnikova, 2015).

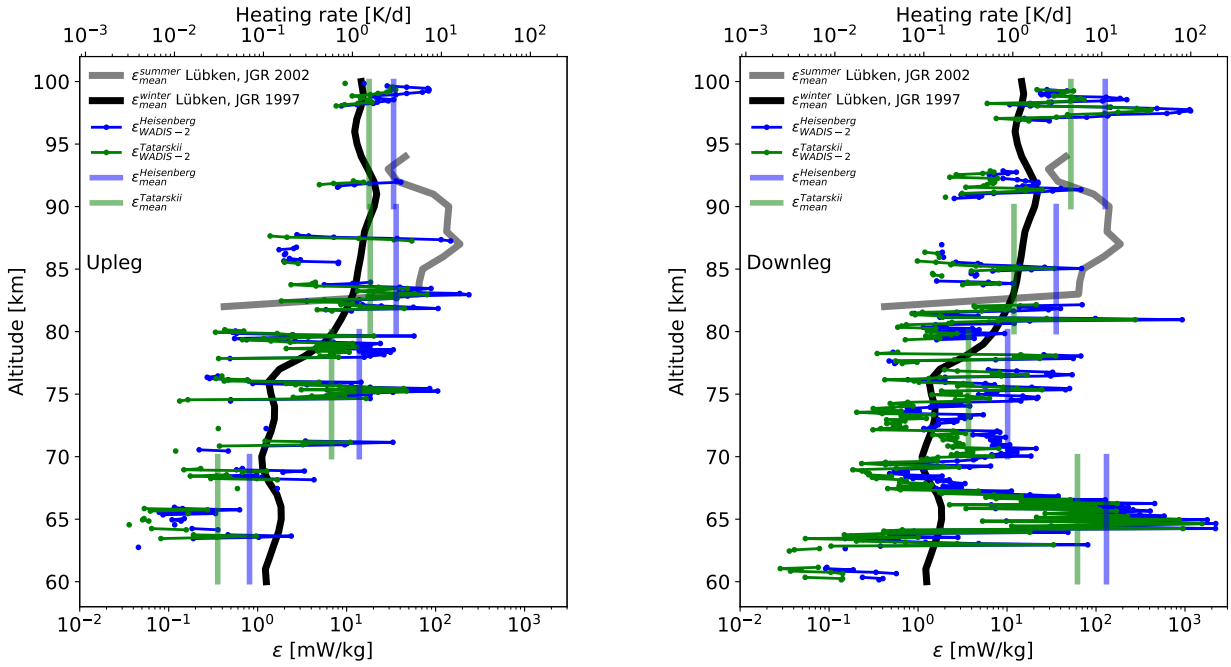

(a) Upleg

(b) Downleg

Figure 12. ~~In situ~~ in-situ turbulence measurements by the WADIS-2 rocket launched on 1st of March 2015 at 01:44:00 UTC. Blue and green colors represent turbulence energy dissipation rates, ε, derived using spectral models of Heisenberg (1948) and Tatarskii (1971), respectively. Vertical lines show mean ε-values over the 10 km height bins. Bold black and gray profiles show turbulence climatologies for winter and summer, respectively.

In Fig. 13 we show wavelet spectrogram of neutral density fluctuations shown in Fig. 11. This spectrum was used to derive the ε-profile shown in Fig. 12b (see Strelnikov et al., 2003, for details). We note that qualitatively similar picture in terms of turbulent structures could be inferred by analyzing the upleg data which is not shown here. In this spectrogram (Fig. 13) power falls down along the spatial scale axis from large to small scales. Noise level corresponds to bluish colors. Turbulent layers can be recognized in this figure as regions of green color which are extended to small-scales of the order of 100 m and less. Note ~~,~~ that this only gives a rough approximate visualization of the turbulence structure. A more close and detailed examination of individual spectra (~~PSD~~ power spectral densities, PSD, vs frequency) is required to derive the ε-profile. Nevertheless, colored wavelet spectrograms like those shown in Fig. 13 help to identify power change at different scales in the spectrum. So, one can identify, for instance, two near parallel slopes in red color between ~80 an ~98 km that extend approximately from scales of 5 to 3 km down to 1 km and slightly below. This region is marked with the blue dashed oval and tilted dashed lines in Fig. 13. This picture is reminiscent of a GW-saturation process when vertical wavelength of GW becomes shorter

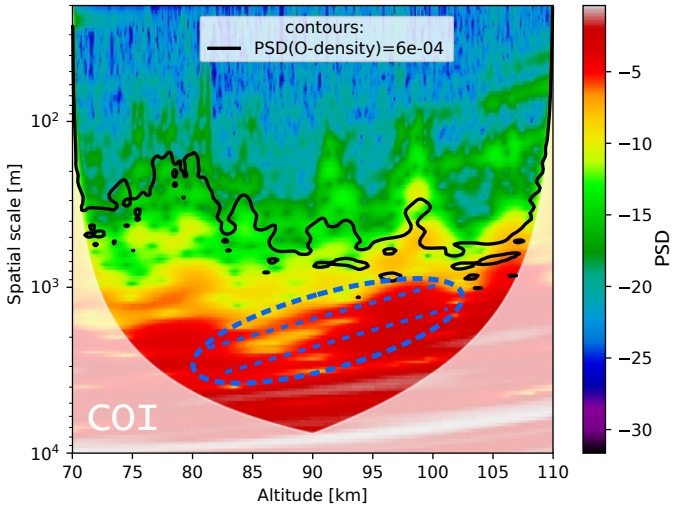

Figure 13. Wavelet spectrum of neutral density fluctuations as color contours. Black contour shows a constant-power line taken from wavelet spectrum of atomic oxygen density fluctuations (not shown here). White shading shows cone of influence (COI). Dashed oval and two lines mark region where power peak shifts from large to small-scales which can be attributed to a GW-saturation process.

(see, e.g., Fig. 5.3 in Nappo, 2002). Consistently, we observed a turbulence layer on top of this saturation region, i.e. in 98 to 100 km range.

In Fig. 13 we further compare the neutral density spectrum derived from the CONE measurements with the spectrum of atomic oxygen density fluctuations derived from the FIPEX measurements. The black contour on top of the colored scalogram is a constant power line taken from a similarly derived wavelet spectrum (not shown here) of the O-density fluctuations which are shown in Fig. 11. The PSD-value that represents the O-spectra (black line) lies well withing inertial subrange (i.e., $k^{-5/3}$ part) inside the regions where turbulence was observed. The contour line reproduces the small-scale structure of neutral density fluctuations quite well. So, all regions where neutral density structures extent to small-scales are also present in the O-density spectra. This suggests that atomic oxygen is affected by turbulent mixing.

In order to directly compare the spectral content of neutral air and atomic oxygen fluctuations we further show in Fig. 14 two dimensional slices of the corresponding wavelet spectrograms (i.e., for neutrals and oxygen). Fig. 14 shows spectra of neutrals and O in black and blue colors, respectively. Additionally, in Fig. 14a we show a Fourier spectrum of the horizontal wind fluctuations (magenta color) shown in Fig. 10. The wind spectrum only extends to ∼200 m which is due to the limited altitude resolution of these measurements. The red dashed line marks slope of k^{-3} (k is wavenumber) which is commonly attributed to gravity waves (Fritts and Alexander, 2003). It is clearly seen that the spectrum of wind fluctuations closely follows the k^{-3} power law. Spectrum of neutrals is also very close to it down to ∼15 m scales where white nose produced by instrument electronics dominates the signal. The spectrum of the instrumental noise is marked in Fig. 14 by a bold gray horizontal line. Dashed green line in Fig. 14a marks $k^{-5/3}$ slope, that is the famous Kolmogorov power law which suggests that turbulence was acting on tracer distribution. It can be seen that the spectrum of O-density fluctuations might have been affected by turbulence.

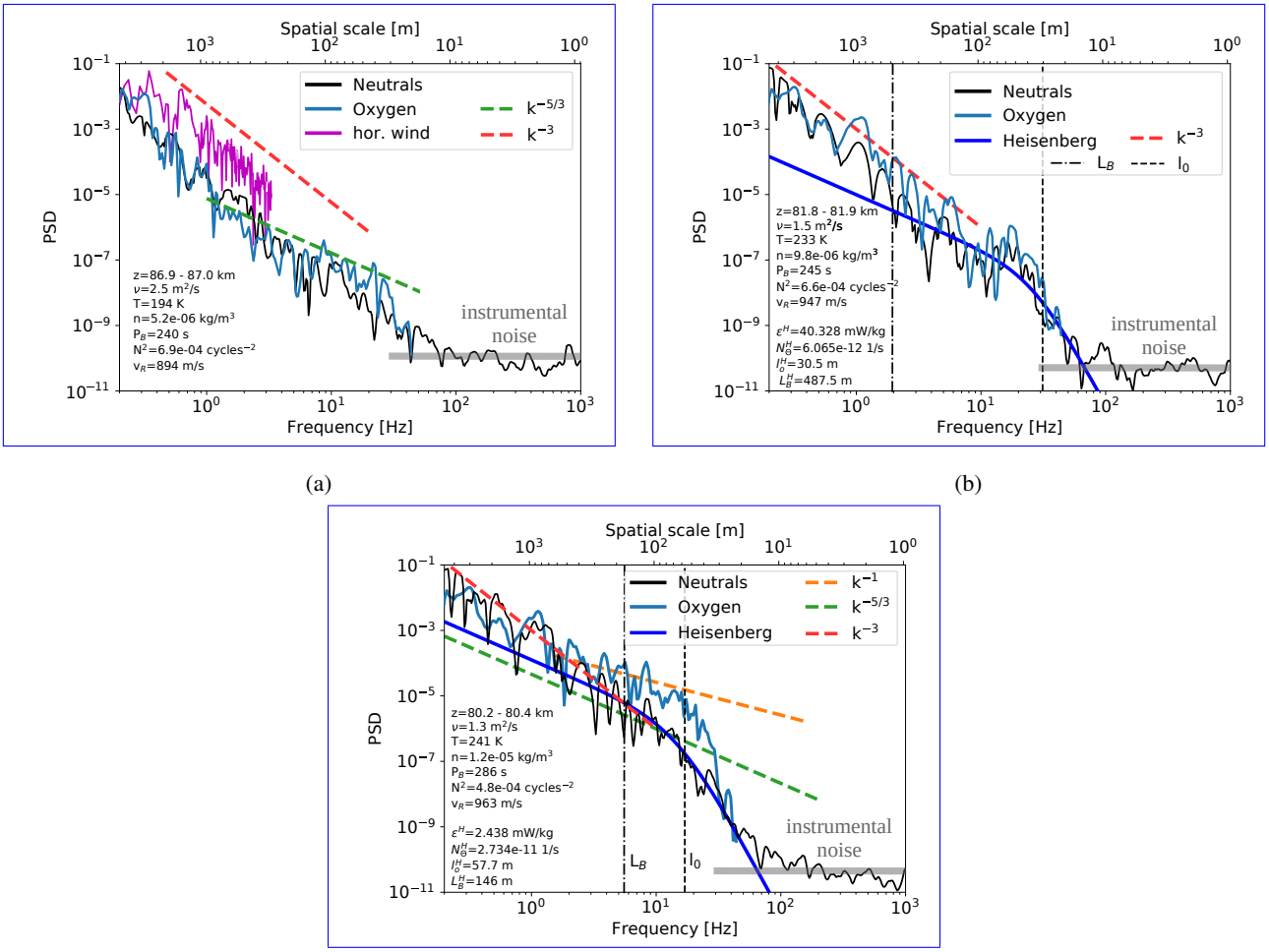

Figure 14. Normalized power spectral densities (PSD) of horizontal wind fluctuations (magenta), $\Delta N_n/N_n$ (black), and $\Delta[O]/[O]$ (blue) measured during descend of WADIS-2 sounding rocket. Dashed red, green, and orange lines show slopes with k^{-3}, $k^{-5/3}$, and k^{-1} power law, respectively. Vertical black dashed and dashed-dotted lines mark inner and buoyancy scales of turbulence, $l_\circ$ and L_B, respectively. Bold gray horizontal lines mark instrumental noise. a) All spectra reveal k^{-3} slope attributed to gravity waves; b) All spectra reveal both waves and turbulence. The neutral- and O-spectrum are near identical. c) Small-scale part of the O-spectrum reveal a k^{-1} slope.

Fig. 14b shows spectra of neutral and oxygen density fluctuations taken from the region where moderate turbulence was observed near 82 km. Dark blue solid bold line also shows the fitted theoretical model of Heisenberg (1948). This model only describes two parts (or subranges) of turbulence spectrum. Its left part called inertial subrange follows the $k^{-5/3}$ power law whereas the dissipation part often referred to as viscous subrange is described by k^{-7} slope. One can see that the leftmost part of both spectra (i.e., for O and neutrals) follows the k^{-3}, i.e. GW-like slope (also marked by red dashed line) which then smoothly transits into the turbulence spectrum well described by the Heisenberg model. The inertial subrange of both spectra spans over the same range of spatial scales, namely from $L_B \approx 500$ down to $l_\circ \approx 30$ m. We recall here, that the ε-value is directly derived from the spatial scale $l_\circ$ defined as transition between inertial and viscous subranges.

Fig. 14c shows spectra from region just below that one described above. The ε-value here drops by one order of magnitude and the inertial subrange shrinks to $\sim$100 m. Interestingly, the atomic oxygen spectrum reveals a somewhat different shape. Fig. 14b and 14c demonstrate two types of spectral behavior of O-density fluctuations inside turbulence layers observed during WADIS-2 rocket experiment.

5 Discussion

In this section we discuss the shown above fluctuations in different quantities measured with rocket-borne and ground-based instruments. First we focus on the large scale morphology in temperature field. Then we discuss fluctuations which might be attributed to gravity waves. Finally, we consider the observed smallest-scale structures due to turbulence.

Fig. 7 shows a prominent temperature enhancement around $\sim$100 km altitude. As mentioned in Sec. 3, Szewczyk et al. (2013) observed similar temperature enhancement in the same altitude region. They showed, that this signature was observed by MLS satellite instrument over large region and was also seen in lidar data for long time. These two facts lead them to conclude that the observed temperature enhancement could be qualified as mesospheric inversion layer (MIL). Their lidar temperature measurements also showed that MIL descended together with tide. A striking feature accompanied MIL studied by Szewczyk et al. (2013) was a very strong turbulence layer with ε=2 W/kg (equivalent to a heating rate of 200 K/day) observed on top of their upper MIL. Interestingly, our downleg data reveal very similar situation. Namely, on top of the temperature enhancement we also observe a vigorous turbulence layer with $\varepsilon \simeq 1$ W/kg (or $\sim$100 K/d). ~~This temperature enhancement~~ Our temperature enhancement (compare Fig. 7 and 3) also descends within a time period of several hours. Their temporal behavior is studied in Wörl et al. (2019), who found dominant periods of 24, 12, and 8 hours. Its spatial extent is at least 60 km (distance between ascent and descent of the sounding rocket plus the distance to the south-east Na-lidar beam, see Fig. 1). The upleg rocket data, however, are somewhat different. ~~They~~ While the upleg measurements show similar temperature enhancement, ~~but the turbulence~~ the turbulence observed is one order of magnitude weaker. Szewczyk et al. (2013) argued that if turbulence itself did not produce the MIL, it might have amplified it. This statement is consistent with our observations. The ~~weaker turbulence on upleg accompany~~ local temperature maximum near 100 km reveal $\sim$10 K ~~colder temperature maximum.~~lower values for upleg measurements than for downleg (see Fig. 7). Also turbulent energy dissipation rates measured on upleg show $\sim$one oder of magnitude lower values than those observed during rocket descend (Fig. 12).

In the previous sections we showed ground-based wind and in-situ density and temperature measurements which reveal signatures of gravity waves. Closer comparison of density fluctuations of neutral gas, positive ions, and atomic oxygen in Fig. 11 shows at least two things. First, the amplitudes of GW in these tracers are different. Second, the phases can be shifted relative to each other. Fritts and Thrane (1990) and Thrane et al. (1994) studied the relationship between ion and neutral density fluctuations due to gravity wave and turbulent motions both theoretically and experimentally. Their results indicated that this relationship in the middle atmosphere ranges between an adiabatic and a chemical equilibrium limit, depending on the characteristics of the wave or turbulent motion and the ion production and recombination rates. In pure adiabatic limit case, that is when fully developed turbulence dominates in observed timeseries, the neutral and ion density fluctuations must be in anti-phase, i.e. shifted by π relative to each other. Fritts and Thrane (1990) also noted that we should not expect the fluctuations of ions and neutrals to be either in or out of phase. Rather, they will have a phase shift that depends on the relative values of the intrinsic wave frequency, the mean ion number density, and the effective recombination rate.

Fritts and Thrane (1990) showed that the phase shift between fluctuations of different species depends on the relative magnitudes of wave and chemistry time scales. For low frequency waves this phase shift $\rightarrow 0$, indicating that the species are in chemical equilibrium. This situation is well observed just above the MIL-like temperature enhancement in the altitude range from 102 to 110 km (see Fig. 11), where all three species, i.e. oxygen, ions, and neutrals show nearly the same oscillations. This behavior is observed directly above the upper turbulence layer measured by rocket-borne instruments on both up- and downleg.

Next, we focus on the feature seen in the wavelet scalogram (Fig. 13) which is marked by the dashed lines. It suggests that waves with vertical wavelength of $\sim$2–3 km saturated within altitude range $\sim$80 to 98 km and broke producing turbulence layers (Fig. 12). That is, our new measurements suggest that turbulence produced by breaking GW amplifies temperature fluctuations producing MIL-like signature in temperature field. Note ~~,~~ that density fluctuations in Fig. 11 do not have this large MIL-like signature because of the background subtraction procedure which filtered out waves longer than 5 km.

It is interesting to note ~~,~~ that also the altitude region below $\sim$82 km reveals feature, similar to what is observed near 100 km height: stronger turbulence activity on downleg accompanies higher temperatures. Furthermore, right above this active region GW-amplitudes seen in temperature data (Fig. 7) are very low. ε-profiles (Fig. 12) also demonstrate lower turbulence activity (which might be connected to low GW-amplitudes). Also wind fluctuations (Fig. 10) are consistent with this picture. Their amplitude grows in the height region 30 to 70 km and afterwards, near 85 km it vanishes.

All these facts together suggest that we observed waves saturation and dissipation in the altitude range 70 to 80 km accompanied by turbulence production. Above these heights we observed GW-amplitude growth and breakdown near 100 km. The latter can be either attributed to secondary GW generated by turbulence (see e.g., Becker and Vadas, 2018, and references therein) or just another wave package passing through our observation field.

The spatial scales considered in the discussion above are of the order of 1 to few kilometers. This range of vertical scales is characteristic for GW in MLT. If we look at these fluctuations in spectral domain (e.g., shown in Fig 14) we see that they follow the k^{-3} slope~~(~~, usually attributed to GW ~~)~~(see e.g., Smith et al., 1987; Weinstock, 1990; Fritts and Alexander, 2003; Žagar et al., 2017, and , in the range of scales from 5 km down to hundreds of meters. Now we discuss structures at smaller scales. A power increase

in spectrum which appears at spatial scales below ∼500 m must rather be attributed to action of turbulence. If the spectrum reveals a clear shape which can be mathematically described by a model (e.g., Heisenberg, 1948; Tatarskii, 1971) we argue that we observed an active turbulence and derive its energy dissipation rate, ε. To do so, we have to make sure, that the density fluctuations that we use for turbulence analysis are passive, that is do not influence the flow and conservative, i.e. its value is not affected by the flow (see e.g., Lübken, 1992, 1997; Lübken et al., 1993, 2002). It was also shown, that plasma density fluctuations can both satisfy this requirement and, under specific conditions, can be affected by non-turbulent processes like enhanced recombination of electrons with cluster ions (e.g., Röttger and La Hoz, 1990), the effect of charged ice particles in PMSE (e.g., Cho et al., 1992), or plasma instabilities (e.g., Blix et al., 1994; Strelnikov et al., 2009). If spectra at small-scales reveal some enhanced power which cannot be described by a model, it might imply that we observed a residual structuring after action of turbulence some time before. In such a case we cannot derive any parameter of turbulence from this data.

Recalling to above discussion about relationship between density fluctuations of neutrals and ions we note that our analysis results suggest that a similar relationship should also exist between small-scale atomic oxygen density fluctuations and other constituents, i.e. ionospheric plasma and neutral gas. So, e.g., earlier common volume rocket-borne measurements of atomic oxygen and electron densities (N_e) by Friedrich et al. (1999) showed a clear correlation between fine structure of O- and N_e-density profiles.

In the height range from ∼78 to ∼85 km in Fig. 11 fluctuations of ion density are in phase with those of O-density and they both are almost in anti-phase with the neutrals. This might imply that we here observed O-densities which are in chemical equilibrium with ion densities (phase shift close to zero) located inside turbulence layers (phase shift $\sim \pi$). The turbulence measurements indeed show turbulent layers in this altitude range (see Fig 12b). On the one hand, this supports the theory of Fritts and Thrane (1990), but at the same time it raises the question how O-density behaves inside turbulence and whether turbulence affects the height distribution of atomic oxygen.

Now we discuss the power spectra shown in Fig. 14. This figure demonstrates three types of spectra found in the fluctuations measured during the WADIS-2 flight. As noted above, the upper panel shows spectra typical for gravity waves whereas two lower panels demonstrate turbulent spectra. The both spectra in the middle panel, i.e. the PSD($\Delta N_n/N_n$) and the PSD(Δ[O]/[O]) shown with black and blue lines, respectively, are near identical, suggesting that at these altitudes the chemical time constant is larger than the turbulent one. At the same time, just below this height, that is where the chemical time constant is expected to be comparable, the PSD(Δ[O]/[O]) shows different spectral behavior revealing a k^{-1} slope at small-scales.

Detailed analysis of all the regions where different types of O-density spectra occur is rather difficult because of different reasons. One reason is that when turbulence is very strong, its spectrum extends down to scales below current FIPEX resolution limit of ∼20 m, that is the O-density spectrum appears not fully resolved. So far we can only identify three regions where third type of spectra (like in Fig. 14c) was observed in the downleg measurements: between 90.9–91.2 km, 80.2–80.4 km, and 81.1–81.7 km.

Friedrich (2016) noted, that O-density should positively correlate with N_e for two reasons: (1) [O] inhibits the formation of water cluster ions (e.g., $H^+(H_2O)_n$) which have significantly faster recombination rates than molecular ions (O_2^+, NO^+) (2) [O]

provides a reverse reaction effectively detaching electrons from negative ions. In terms of density fluctuations, N_e is ultimately connected to the ambient ion density, N_i, which, in turn at heights below $\sim$100 km are essentially governed by collisions with neutrals (e.g., Rapp et al., 2003). That is the small-scale structures produced by turbulence must be observed in these species too. The difference in their response to turbulence arise due to difference of their diffusivity. Thus, diffusion constant of charged constituents is affected by ambipolar forces resulting from electrostatic coupling between positively and negatively charged species (e.g., Chen, 2016). Moreover, it was shown that heavy charged aerosols if present can significantly reduce plasma diffusivity allowing extension of eddy cascade in those species down to much smaller scales (e.g., Rapp et al., 2003). This, for instance can lead to such phenomena like polar mesosphere radar echoes in summer or winter, PMSE or PMWE, respectively (see e.g., Rapp and Lübken, 2004; Lübken et al., 2006). Under conditions when diffusivity, D, of plasma species is considerably reduced its spectral behavior can be described by a model which includes this parameter via e.g., Schmidt number, Sc=ν/D, where ν is kinematic viscosity of ambient gas (e.g., Driscoll and Kennedy, 1985). Such models implement theory of Batchelor (1958) and describe the small-scale part of the spectrum by a k^{-1} power law. In other words, if spectrum of density fluctuations reveals the k^{-1} slope at scales smaller than those where $k^{-5/3}$ is present, this means that the diffusivity of this constituent is reduced. To summarize, spectra of O-density fluctuations which show the k^{-1} slope (one example of those is shown in Fig. 14c), may imply that atomic oxygen can show different diffusion properties inside turbulence layers. That is, addressing the question whether turbulence affects height distribution of atomic oxygen, we can definitely say yes. The observed k^{-1} spectral behavior, however needs further in depth investigation and lies out of scope of this paper.

6 Conclusions

In this paper we present an overview of the entire scope of measurements conducted in the frame of the WADIS-2 sounding rocket campaign. We also demonstrate the important role of small-scale processes like gravity waves and turbulence in the distribution of O in the MLT region.

We show that all measured quantities, including winds, densities, and temperatures, reveal signatures of both waves and turbulence. Analysis of density fluctuations measured by rocket-borne instruments supported the theory by Fritts and Thrane (1990), but also suggested that a similar relationship might exist between atomic oxygen and other constituents, i.e., plasma and neutrals.

Atomic oxygen inside turbulent layers showed two different spectral behaviors at scales smaller than $\sim$300 m. Some of the O-density spectra reproduce spectra of neutral gas, but some of them show a k^{-1} slope. A more detailed study of such very small scales in O-density data is subject of our future work. In particular, a somewhat higher altitude resolution and enhanced sensitivity of FIPEX sensors may yield more detailed picture for our future rocket experiments.

Author contributions. M.R., F.J.L. and B.S. designed and directed the project; B.S., M.F., R.L., J.H., M.K., J.G., S.L., S.F., G.B., J.H., A.B., M.J.T. designed and directed the subprojects and related instruments; M.E., M.F., J.H., M.K., G.B., B.P.W., H.A., R.L., J.H., R.W., A.B.,

M.J.T, P.D.P performed the experiments; B.S., M.E., M.F., J.H., G.B., B.P.W., T.S., H.A., I.S., R.L., M.G., J.H., R.W., A.B., M.J.T, P.D.P analyzed the data; All authors contributed to the final manuscript.

Competing interests. The authors declare that they have no conflict of interest.

Acknowledgements. This work was supported by the German Space Agency (DLR) under grant 50 OE 1001 (Project WADIS). Authors thank DLR-MORABA for their excellent contribution to the project by developing the complicated WADIS payloads and campaigns support together with the Andøya Space Center. Authors thank H.-J. Heckl and T. Köpnick for building the IAP rocket instrumentation. The design and initial development of the AMTM was supported under an AFOSR DURIP grant to USU. The AMTM installation and operations at ALOMAR were supported under the NSF collaborative grant AGS-1042227. The sodium lidar observations and data analysis were supported by NSF grants AGS-1136269, AGS-1734693, and AGS-1829138.

References

Alexander, M. J., Geller, M., McLandress, C., Polavarapu, S., Preusse, P., Sassi, F., Sato, K., Eckermann, S., Ern, M., Hertzog, A., Kawatani, Y., Pulido, M., Shaw, T. A., Sigmond, M., Vincent, R., and Watanabe, S.: Recent developments in gravity-wave effects in climate models and the global distribution of gravity-wave momentum flux from observations and models, Quarterly Journal of the Royal Meteorological Society, 136, 1103–1124, https://doi.org/10.1002/qj.637, https://rmets.onlinelibrary.wiley.com/doi/abs/10.1002/qj.637, 2010.

Arnold, K. S. and She, C. Y.: Metal fluorescence lidar (light detection and ranging) and the middle atmosphere, Contemporary Physics, 44, 35–49, https://doi.org/10.1080/00107510302713, 2003.

Asmus, H., Staszak, T., Strelnikov, B., Lübken, F.-J., Friedrich, M., and Rapp, M.: Estimate of size distribution of charged MSPs measured in situ in winter during the WADIS-2 sounding rocket campaign, Annales Geophysicae, 35, 979–998, https://doi.org/10.5194/angeo-35-979-2017, 2017.

Batchelor, G. K.: Small scale variation of convected quantities like temperature in turbulent field, J. Fluid Mech., 5, 113–133, 1958.

Baumgarten, G.: Doppler Rayleigh/Mie/Raman lidar for wind and temperature measurements in the middle atmosphere up to 80 km, Atmospheric Measurement Techniques, 3, 1509, 2010.

Becker, E. and Schmitz, G.: Energy Deposition and Turbulent Dissipation Owing to Gravity Waves in the Mesosphere., Journal of Atmospheric Sciences, 59, 54–68, https://doi.org/10.1175/1520-0469(2002)059<0054:EDATDO>2.0.CO;2, 2002.

Becker, E. and Vadas, S. L.: Secondary gravity waves in the winter mesosphere: Results from a high-resolution global circulation model, J. Geophys. Res., 123, 2605–2627, https://doi.org/10.1002/2017JD027460, 2018.

Bishop, R. L., Larsen, M. F., Hecht, J. H., Liu, A. Z., and Gardner, C. S.: TOMEX: Mesospheric and lower thermospheric diffusivities and instability layers, Journal of Geophysical Research: Atmospheres, 109, https://doi.org/10.1029/2002JD003079, https://agupubs.onlinelibrary.wiley.com/doi/abs/10.1029/2002JD003079, 2004.

Blix, T. A., Thrane, E. V., Kirkwood, S., and Schlegel, K.: Plasma instabilities in the lower E-region observed during the DYANA campaign, J. Atmos. Terr. Phys., 56, 1853–1870, 1994.

Caridade, P. J. S. B., Horta, J.-Z. J., and Varandas, A. J. C.: Implications of the O + OH reaction in hydroxyl nightglow modeling, Atmospheric Chemistry & Physics, 13, 1–13, https://doi.org/10.5194/acp-13-1-2013, 2013.

Chen, F. F.: Introduction to Plasma Physics and Controlled Fusion, https://doi.org/10.1007/978-3-319-22309-4, 2016.

Cho, J. Y. N., Hall, T. M., and Kelley, M. C.: On the role of charged aerosols in polar mesosphere summer echoes, J. Geophys. Res., 97, 875–886, 1992.

Driscoll, R. J. and Kennedy, L. A.: A model for the spectrum of passive scalars in an isotropic turbulence field, Phys. Fluids, 28, 72–80, 1985.

Eberhart, M., Löhle, S., Steinbeck, A., Binder, T., and Fasoulas, S.: Measurement of atomic oxygen in the middle atmosphere using solid electrolyte sensors and catalytic probes, Atmospheric Measurement Techniques, 8, 3701–3714, https://doi.org/10.5194/amt-8-3701-2015, 2015.

Eberhart, M., Löhle, S., Strelnikov, B., , Fasoulas, S., Lübken, F.-J., Rapp, M., Hedin, J., Khaplanov, M., and Gumbel, J.: Atomic oxygen number densities in the MLT region measured by solid electrolyte sensors on WADIS-2, Atmospheric Measurement Techniques, submitted, this issue, 2018.

Egito, F., Takahashi, H., and Miyoshi, Y.: Effects of the planetary waves on the MLT airglow, Annales Geophysicae, 35, 1023–1032, https://doi.org/10.5194/angeo-35-1023-2017, https://www.ann-geophys.net/35/1023/2017/, 2017.

Feofilov, A. G. and Kutepov, A. A.: Infrared Radiation in the Mesosphere and Lower Thermosphere: Energetic Effects and Remote Sensing, Surveys in Geophysics, 33, 1231–1280, https://doi.org/10.1007/s10712-012-9204-0, https://doi.org/10.1007/s10712-012-9204-0, 2012.

Fomichev, V. I., Ogibalov, V. P., and Beagley, S. R.: Solar heating by the near-IR CO2 bands in the mesosphere, Geophysical Research Letters, 31, https://doi.org/10.1029/2004GL020324, https://agupubs.onlinelibrary.wiley.com/doi/abs/10.1029/2004GL020324, 2004.

Friedrich, M.: Handbook of the Lower Ionosphere, Verlag der Technischen Universität Graz, https://doi.org/10.3217/ 978-3-85125-485-3, https://lampx.tugraz.at/~karl/verlagspdf/ionosphere_friedrich_ebook.pdf, 2016.

Friedrich, M. and Torkar, K.: High-latitude plasma densities and their relation to riometer absorption, Journal of Atmospheric and Terrestrial Physics, 45, 127 – 135, https://doi.org/https://doi.org/10.1016/S0021-9169(83)80017-8, http://www.sciencedirect.com/science/article/pii/S0021916983800178, 1983.

Friedrich, M., Gumbel, J., and Pilgram, R.: Atomic Oxygen in the Mesosphere and its Relevance for the Ionosphere: A Summary of Empirical Evidence, in: European Rocket and Balloon Programs and Related Research, edited by Kaldeich-Schürmann, B., vol. 437 of *ESA Special Publication*, p. 287, 1999.

Fritts, D. C. and Alexander, M. J.: Gravity wave dynamics and effects in the middle atmosphere, Reviews of Geophysics, 41, 1003, https://doi.org/10.1029/2001RG000106, 2003.

Fritts, D. C. and Thrane, E. V.: Computation of the ion/neutral density ratio in the presence of wave and chemical effects, Journal of Atmospheric and Terrestrial Physics, 52, 827–834, https://doi.org/10.1016/0021-9169(90)90019-J, 1990.

Fritts, D. C., Pautet, P.-D., Bossert, K., Taylor, M. J., Williams, B. P., Iimura, H., Yuan, T., Mitchell, N. J., and Stober, G.: Quantifying gravity wave momentum fluxes with Mesosphere Temperature Mappers and correlative instrumentation, Journal of Geophysical Research (Atmospheres), 119, 13, https://doi.org/10.1002/2014JD022150, 2014.

Fukao, S., Yamanaka, M., Ao, N., K Hocking, W., Sato, T., Yamamoto, M., Nakamura, T., Tsuda, T., Kato, S., and , b.: Seasonal variability of vertical eddy diffusivity in the middle atmosphere 1. Three-year observations by the middle and upper atmosphere radar, Journal of Geophysical Research, 99, 18 973–18 987, https://doi.org/10.1029/94JD00911, 1994.

Grygalashvyly, M., Eberhart, M., Hedin, J., Strelnikov, B., Lübken, F.-J., Rapp, M., Löhle, S., Fasoulas, S., Khaplanov, M., Gumbel, J., and Vorobeva, E.: Atmospheric band fitting coefficients derived from a self-consistent rocket-borne experiment, Atmospheric Chemistry and Physics, 19, 1207–1220, https://doi.org/10.5194/acp-19-1207-2019, https://www.atmos-chem-phys.net/19/1207/2019/, 2019.

Gumbel, J.: Aerodynamic influences on atmospheric in situ measurements from sounding rockets, Journal of Geophysical Research: Space Physics, 106, 10 553–10 563, https://doi.org/10.1029/2000JA900166, https://agupubs.onlinelibrary.wiley.com/doi/abs/10.1029/2000JA900166, 2001.

Gumbel, J., Rapp, M., and Unckell, C.: Aerodynamic Aspects of Rocket-Borne in situ Studies, in: European Rocket and Balloon Programs and Related Research, edited by Kaldeich-Schürmann, B., vol. 437 of *ESA Special Publication*, p. 459, 1999.

Hauchecorne, A. and Chanin, M.-L.: Density and temperature profiles obtained by lidar between 35 and 70 km, Geophys. Res. Lett., 7, 565–568, https://doi.org/10.1029/GL007i008p00565, 1980.

Hedin, J., Gumbel, J., and Rapp, M.: On the efficiency of rocket-borne particle detection in the mesosphere, Atmospheric Chemistry and Physics, 7, 3701–3711, https://doi.org/10.5194/acp-7-3701-2007, https://www.atmos-chem-phys.net/7/3701/2007/, 2007.

Hedin, J., Gumbel, J., Stegman, J., and Witt, G.: Use of O_2 airglow for calibrating direct atomic oxygen measurements from sounding rockets, Atmospheric Measurement Techniques, 2, 801–812, 2009.

Heisenberg, W.: Zur statistischen Theorie der Turbulenz, Z. Physik, 124, 628–657, 1948.

Hines, C. O. and Tarasick, D. W.: On the detection and utilization of gravity waves in airglow studies, Planetary and Space Science, 35, 851–866, https://doi.org/10.1016/0032-0633(87)90063-8, 1987.

Höffner, J. and Fricke-Begemann, C.: Accurate lidar temperatures with narrowband filters, Opt. Lett., 30, 890–892, https://doi.org/10.1364/OL.30.000890, http://ol.osa.org/abstract.cfm?URI=ol-30-8-890, 2005.

Höffner, J. and Lautenbach, J.: Daylight measurements of mesopause temperature and vertical wind with the mobile scanning iron lidar, Opt. Lett., 34, 1351–1353, https://doi.org/10.1364/OL.34.001351, http://ol.osa.org/abstract.cfm?URI=ol-34-9-1351, 2009.

Latteck, R. and Bremer, J.: Long-term variations of polar mesospheric summer echoes observed at Andøya (69°N), Journal of Atmospheric and Solar-Terrestrial Physics, 163, 31 – 37, https://doi.org/https://doi.org/10.1016/j.jastp.2017.07.005, http://www.sciencedirect.com/science/article/pii/S1364682617300846, long-term changes and trends in the upper atmosphere, 2017.

Latteck, R. and Strelnikova, I.: Extended observations of polar mesosphere winter echoes over Andøya (69°N) using MAARSY, Journal of Geophysical Research (Atmospheres), 120, 8216–8226, https://doi.org/10.1002/2015JD023291, 2015.

Latteck, R., Singer, W., Rapp, M., Vandepeer, B., Renkwitz, T., Zecha, M., and Stober, G.: MAARSY: The new MST radar on Andøya-System description and first results, Radio Science, 47, RS1006, https://doi.org/10.1029/2011RS004775, 2012.

Lautenbach, J. and Höffner, J.: Scanning iron temperature lidar for mesopause temperature observation, Appl. Opt., 43, 4559–4563, https://doi.org/10.1364/AO.43.004559, http://ao.osa.org/abstract.cfm?URI=ao-43-23-4559, 2004.

Lednyts'kyy, O., von Savigny, C., Eichmann, K.-U., and Mlynczak, M. G.: Atomic oxygen retrievals in the MLT region from SCIAMACHY nightglow limb measurements, Atmospheric Measurement Techniques, 8, 1021–1041, https://doi.org/10.5194/amt-8-1021-2015, 2015.

Lübken, F.-J.: On the extraction of turbulent parameters from atmospheric density fluctuations, J. Geophys. Res., 97, 20,385–20,395, 1992.

Lübken, F.-J.: Seasonal variation of turbulent energy dissipation rates at high latitudes as determined by insitu measurements of neutral density fluctuations, J. Geophys. Res., 102, 13,441–13,456, 1997.

Lübken, F.-J., Hillert, W., Lehmacher, G., and von Zahn, U.: Experiments revealing small impact of turbulence on the energy budget of the mesosphere and lower thermosphere, J. Geophys. Res., 98, 20,369–20,384, 1993.

Lübken, F.-J., Rapp, M., and Hoffmann, P.: Neutral air turbulence and temperatures in the vicinity of polar mesosphere summer echoes, J. Geophys. Res., 107(D15), 4273–4277, https://doi.org/10.1029/2001JD000 915, 2002.

Lübken, F.-J., Strelnikov, B., Rapp, M., Singer, W., Latteck, R., Brattli, A., Hoppe, U.-P., and Friedrich, M.: The thermal and dynamical state of the atmosphere during polar mesosphere winter echoes, Atmos. Chem. Phys., 6, 13–24, 2006.

Lübken, F.-J., Berger, U., and Baumgarten, G.: Temperature trends in the midlatitude summer mesosphere, Journal of Geophysical Research (Atmospheres), 118, 13, https://doi.org/10.1002/2013JD020576, 2013.

Marsh, D. R., Smith, A. K., Mlynczak, M. G., and Russell, J. M.: SABER observations of the OH Meinel airglow variability near the mesopause, Journal of Geophysical Research (Space Physics), 111, A10S05, https://doi.org/10.1029/2005JA011451, 2006.

McDade, I. C.: The photochemistry of the MLT oxygen airglow emissions and the expected influences of tidal perturbations, Advances in Space Research, 21, 787–794, https://doi.org/10.1016/S0273-1177(97)00674-1, 1998.

McDade, I. C., Murtagh, D. P., Greer, R. G. H., Dickinson, P. H. G., Witt, G., Stegman, J., Llewellyn, E. J., Thomas, L., and Jenkins, D. B.: ETON 2 - Quenching parameters for the proposed precursors of O2(b1Sigma + g) and O(1S) in the terrestrial nightglow, Planetary and Space Science, 34, 789–800, https://doi.org/10.1016/0032-0633(86)90075-9, 1986.

McKinnell, L.-A. and Friedrich, M.: A neural network-based ionospheric model for the auroral zone, Journal of Atmospheric and Solar-Terrestrial Physics, 69, 1459–1470, https://doi.org/10.1016/j.jastp.2007.05.003, 2007.

Mlynczak, M. G. and Solomon, S.: Middle atmosphere heating by exothermic chemical reactions involving odd-hydrogen species, Geophysical Research Letters, 18, 37–40, https://doi.org/10.1029/90GL02672, https://agupubs.onlinelibrary.wiley.com/doi/abs/10.1029/90GL02672, 1991.

Mlynczak, M. G. and Solomon, S.: A detailed evaluation of the heating efficiency in the middle atmosphere, J. Geophys. Res., 98, 10, https://doi.org/10.1029/93JD00315, 1993.

Nappo, C. J.: An introduction to atmospheric gravity waves, 2002.

Pautet, P.-D., Taylor, M. J., Pendleton, W. R., Zhao, Y., Yuan, T., Esplin, R., and McLain, D.: Advanced mesospheric temperature mapper for high-latitude airglow studies, Appl. Optics, 53, 5934, https://doi.org/10.1364/AO.53.005934, 2014.

Picone, J. M., Hedin, A. E., Drob, D. P., and Aikin, A. C.: NRLMSISE-00 empirical model of the atmosphere: Statistical comparisons and scientific issues, Journal of Geophysical Research (Space Physics), 107, 1468, https://doi.org/10.1029/2002JA009430, 2002.

Rapp, M. and Lübken, F.-J.: Polar mesosphere summer echoes (PMSE): Review of observations and current understanding, Atmos. Chem. Phys., 4, 2601–2633, 2004.

Rapp, M., Gumbel, J., and Lübken, F.-J.: Absolute density measurements in the middle atmosphere, Ann. Geophys., 19, 571–580, 2001.

Rapp, M., Lübken, F.-J., and Blix, T. A.: Small scale density variations of electrons and charged particles in the vicinity of polar mesosphere summer echoes, Atmospheric Chemistry and Physics, 3, 1399–1407, https://doi.org/10.5194/acp-3-1399-2003, https://www.atmos-chem-phys.net/3/1399/2003/, 2003.

Rapp, M., Strelnikov, B., Müllemann, A., Lübken, F.-J., and Fritts, D. C.: Turbulence measurements and implications for gravity wave dissipation during the MaCWAVE/MIDAS rocket program, Geophys. Res. Lett., 31, L24S07, https://doi.org/10.1029/2003GL019325, 2004.

Rapp, M., Latteck, R., Stober, G., Hoffmann, P., Singer, W., and Zecha, M.: First three-dimensional observations of polar mesosphere winter echoes: Resolving space-time ambiguity, J. Geophys. Res., 116, A11307, https://doi.org/10.1029/2011JA016858, 2011.

Röttger, J. and La Hoz, C.: Characteristics of polar mesosphere summer echoes (PMSE) observed with the EISCAT 224 MHz radar and possible explanations of their origin, Journal of Atmospheric and Terrestrial Physics, 52, 893–906, 1990.

Selvaraj, D., Patra, A. K., and Narayana Rao, D.: On the seasonal variations of reflectivity and turbulence characteristics of low-latitude mesospheric echoes over Gadanki, Journal of Geophysical Research: Atmospheres, 121, 6164–6177, https://doi.org/10.1002/2015JD024283, https://agupubs.onlinelibrary.wiley.com/doi/abs/10.1002/2015JD024283.

She, C. Y., Vance, J. D., Williams, B. P., Krueger, D. A., Moosmüller, H., Gibson-Wilde, D., and Fritts, D.: Lidar studies of atmospheric dynamics near polar mesopause, Eos, Transactions American Geophysical Union, 83, 289–293, https://doi.org/10.1029/2002EO000206, https://agupubs.onlinelibrary.wiley.com/doi/abs/10.1029/2002EO000206.

Smith, A. K., Marsh, D. R., Mlynczak, M. G., and Mast, J. C.: Temporal variations of atomic oxygen in the upper mesosphere from SABER, Journal of Geophysical Research (Atmospheres), 115, D18309, https://doi.org/10.1029/2009JD013434, 2010.

Smith, S. A., Fritts, D. C., and Vanzandt, T. E.: Evidence for a Saturated Spectrum of Atmospheric Gravity Waves., Journal of Atmospheric Sciences, 44, 1404–1410, https://doi.org/10.1175/1520-0469(1987)044<1404:EFASSO>2.0.CO;2, 1987.

Snively, J. B.: Mesospheric hydroxyl airglow signatures of acoustic and gravity waves generated by transient tropospheric forcing, Geophysical Research Letters, 40, 4533–4537, https://doi.org/10.1002/grl.50886, 2013.

Staszak, T., Brede, M., and Strelnikov, B.: Open Source Software Openfoam as a New Aerodynamical Simulation Tool for Rocket-Borne Measurements, in: 22nd ESA Symposium on European Rocket and Balloon Programmes and Related Research, edited by Ouwehand, L., vol. 730 of *ESA Special Publication*, p. 201, 2015.

Strelnikov, B., Rapp, M., and Lübken, F.-J.: A new technique for the analysis of neutral air density fluctuations measured in situ in the middle atmosphere, Geophysical Research Letters, 30, 2052, https://doi.org/doi:10.1029/2003GL018271, 2003.

Strelnikov, B., Rapp, M., Zecha, M., Blix, T. A., Friedrich, M., and Yeoman, T. K.: PMSE and E-region plasma instability: In situ observations, Journal of Atmospheric and Solar-Terrestrial Physics, 71, 143–157, https://doi.org/10.1016/j.jastp.2008.10.003, 2009.

Strelnikov, B., Rapp, M., and Lübken, F.: In-situ density measurements in the mesosphere/lower thermosphere region with the TOTAL and CONE instruments, pp. 1–11, Terrapub, https://doi.org/10.5047/aisi.001, 2013.

Strelnikov, B., Szewczyk, A., Strelnikova, I., Latteck, R., Baumgarten, G., Lübken, F.-J., Rapp, M., Fasoulas, S., Löhle, S., Eberhart, M., Hoppe, U.-P., Dunker, T., Friedrich, M., Hedin, J., Khaplanov, M., Gumbel, J., and Barjatya, A.: Spatial and temporal variability in MLT turbulence inferred from in situ and ground-based observations during the WADIS-1 sounding rocket campaign, Annales Geophysicae, 35, 547–565, https://doi.org/10.5194/angeo-35-547-2017, 2017.

Strelnikova, I., Baumgarten, G., and Lüebken, F.-J.: Advanced hodograph-based analysis technique to derive gravity waves parameters, Atmos. Meas. Tech. Discuss., p. under review, https://www.atmos-meas-tech-discuss.net/amt-2019-79/, ~~, 2018.~~ 2019.

Szewczyk, A., Strelnikov, B., Rapp, M., Strelnikova, I., Baumgarten, G., Kaifler, N., Dunker, T., and Hoppe, U.-P.: Simultaneous observations of a Mesospheric Inversion Layer and turbulence during the ECOMA-2010 rocket campaign, Ann. Geophys., 31, 775–785, https://doi.org/10.5194/angeo-31-775-2013, 2013.

Tatarskii, V. I.: The effects of the turbulent atmosphere on wave propagation, Jerusalem: Israel Program for Scientific Translations, 1971.

Taylor, M. J., Bishop, M. B., and Taylor, V.: All-sky measurements of short period waves imaged in the OI(557.7 nm), Na(589.2 nm) and near infrared OH and O_2(0,1) nightglow emissions during the ALOHA-93 Campaign, Geophysical Research Letters, 22, 2833–2836, https://doi.org/10.1029/95GL02946, 1995.

Taylor, M. J., Pendleton, W. R., Clark, S., Takahashi, H., Gobbi, D., and Goldberg, R. A.: Image measurements of short-period gravity waves at equatorial latitudes, Journal of Geophysical Research, 102, 26, https://doi.org/10.1029/96JD03515, 1997.

Taylor, M. J., Pautet, P.-D., Medeiros, A. F., Buriti, R., Fechine, J., Fritts, D. C., Vadas, S. L., Takahashi, H., and São Sabbas, F. T.: Characteristics of mesospheric gravity waves near the magnetic equator, Brazil, during the SpreadFEx campaign, Annales Geophysicae, 27, 461–472, https://doi.org/10.5194/angeo-27-461-2009, 2009.

Thrane, E. V., Blix, T. A., Hoppe, U.-P., Lübken, F.-J., Hillert, W., Lehmacher, G., and Fritts, D. C.: A study of small-scale waves and turbulence in the mesosphere using simultaneous in situ observations of neutral gas and plasma fluctuations, Journal of Atmospheric and Terrestrial Physics, 56, 1797–1808, https://doi.org/10.1016/0021-9169(94)90011-6, 1994.

Torr, D. G.: The photochemistry of the upper atmosphere, pp. 165–278, 1985.

Žagar, N., Jelić, D., Blaauw, M., and Bechtold, P.: Energy Spectra and Inertia-Gravity Waves in Global Analyses, Journal of Atmospheric Sciences, 74, 2447–2466, https://doi.org/10.1175/JAS-D-16-0341.1, 2017.

von Zahn, U., Thrane, E. V., and Skatteboe, R.: The ALOMAR facility: Status and outlook, in: Proceedings of the 12^{th} ESA Symposium on European Rocket and Balloon Programmes and Related Research, edited by Blix, T. A., vol. ESA SP–370, pp. 379–385, Lillehammer, Norway, 1995.

von Zahn, U., von Cossart, G., Fiedler, J., Fricke, K. H., Nelke, G., Baumgarten, G., Rees, D., Hauchecorne, A., and Adolfsen, K.: The ALOMAR Rayleigh/Mie/Raman lidar: objectives, configuration, and performance, Ann. Geophys., 18, 815–833, https://doi.org/10.1007/s005850000210, 2000.

Walterscheid, R. L., Schubert, G., and Straus, J. M.: A dynamical-chemical model of wave-driven fluctuations in the OH nightglow, Journal of Geophysical Research, 92, 1241–1254, https://doi.org/10.1029/JA092iA02p01241, 1987.

Weinstock, J.: Saturated and Unsaturated Spectra of Gravity Waves and Scale-Dependent Diffusion., Journal of Atmospheric Sciences, 47, 2211–2226, https://doi.org/10.1175/1520-0469(1990)047<2211:SAUSOG>2.0.CO;2, 1990.

Wörl, R., Strelnikov, B., Viehl, T. P., Höffner, J., Pautet, P.-D., Taylor, M., J., Zhao, Y., and Lübken, F.: J.: Thermal structure of the mesopause region during the WADIS-2 rocket campaign, Atmospheric Chemistry and Physics, submitted, 2018. 19, 77–88, https://doi.org/10.5194/acp-19-77-2019, https://www.atmos-chem-phys.net/19/77/2019/, 2019.

Yamada, Y., Fukunishi, H., Nakamura, T., and Tsuda, T.: Breaking of small-scale gravity wave and transition to turbulence observed in OH airglow, Geophysical Research Letters, 28, 2153–2156, https://doi.org/10.1029/2000GL011945, 2001.